NASA TECHNICAL MEMORANDUM

NASA TM X-1097

NASA TM X-1097

STATIC AERODYNAMIC CHARACTERISTICS OF A MODEL OF A HORIZONTAL-TAKE-OFF REUSABLE LAUNCH VEHICLE AT MACH NUMBERS 1.60, 2.16, AND 2.86

by John P. Decker and Larry R. Clark

Langley Research Center
Langley Station, Hampton, Va.

NATIONAL AERONAUTICS AND SPACE ADMINISTRATION • WASHINGTON, D. C. • MAY 1965

NASA TM X-1097

STATIC AERODYNAMIC CHARACTERISTICS OF A MODEL OF A HORIZONTAL-TAKE-OFF REUSABLE LAUNCH VEHICLE AT MACH NUMBERS 1.60, 2.16, AND 2.86

By John P. Decker and Larry R. Clark

Langley Research Center
Langley Station, Hampton, Va.

NATIONAL AERONAUTICS AND SPACE ADMINISTRATION

STATIC AERODYNAMIC CHARACTERISTICS OF A MODEL OF A HORIZONTAL-TAKE-OFF REUSABLE LAUNCH VEHICLE AT MACH NUMBERS 1.60, 2.16, AND 2.86*

By John P. Decker and Larry R. Clark
Langley Research Center

SUMMARY

A wind-tunnel investigation was made at supersonic speeds of an approximate 1/75-scale model of a conceptual multistage horizontal-take-off reusable launch vehicle. The model consisted of a winged reusable first stage with a canard, a winged reusable second stage, and a third-stage winged reusable spacecraft with an expendable maneuver propulsion package. The two upper stages were arranged in tandem, and this combination was placed parallel to the first stage. The model was tested at Mach numbers of 1.60, 2.16, and 2.86, at angles of attack from -4° to 26°, and generally at sideslip angles of 0° and 4°. The test Reynolds number per foot remained constant at 2.5×10^{6}.

For the selected moment reference center, the complete first stage was longitudinally stable at zero lift at Mach numbers of 1.60 and 2.16 but was neutrally stable at a Mach number of 2.86. The complete first stage was found to have at least neutral directional stability and positive effective dihedral over most of the angle-of-attack range and throughout the Mach number range of these tests. The canard was very destabilizing longitudinally but increased effective dihedral and directional stability significantly at high angles of attack. Maximum lift-drag ratios for the complete first stage remained nearly constant at 4.3 throughout the test Mach number range.

Addition of the complete upper stages to the complete first stage caused destabilizing increments both longitudinally and directionally and caused reductions in positive effective dihedral at all test Mach numbers. The complete launch vehicle was longitudinally stable at zero lift only at a Mach number of 1.60. The complete launch vehicle had positive effective dihedral but was directionally unstable at all test Mach numbers. Changing the upper-stage configuration significantly influenced both the longitudinal and directional stability of the complete launch vehicle.

---

*Title, Unclassified.

INTRODUCTION

A research program is being conducted at the Langley Research Center to study some of the aerodynamic problems associated with launch vehicles incorporating reusable components. Results of investigations on models of both horizontal-take-off and vertical-take-off reusable launch vehicles are given in references 1 to 8. The present tests are a continuation into the lower supersonic speed regime of an investigation of a conceptual horizontal-take-off reusable launch vehicle. Static aerodynamic characteristics for this model at subsonic and transonic speeds are reported in reference 6; static aerodynamic and static aerodynamic separation characteristics on a smaller scale model of this vehicle at high supersonic and low hypersonic speeds are reported in references 7 and 8, respectively.

The complete launch vehicle consisted of a winged reusable first stage with a canard, a winged reusable second stage, and a third-stage winged reusable spacecraft with an expendable propulsion package for in-orbit maneuvering. The upper stages were arranged in tandem, and this combination was placed parallel to the first stage. The first-stage canard was incorporated primarily to satisfy the control requirements of the first stage during its reentry phase.

All stages of the vehicle were conceived to employ rocket engines using liquid oxygen and hydrogen propellants during boost. The first stage was assumed to utilize turbojet engines as its return propulsion system during subsonic flight, whereas the second and spacecraft stages were considered to be glide return vehicles.

The launch vehicle was designed to place a maximum of 20,000 pounds of spacecraft into a low earth orbit. The vehicle was assumed to be rocket powered and to perform a rapid pull-up, keeping the total acceleration between 2.5g and 3.0g, to get into a ballistic trajectory and minimize the gravity losses. Stage separation was estimated to occur at a speed of 6500 fps at an altitude of about 230,000 feet, and the take-off wing loading was assumed to be 120 lb/sq ft, based on total wing area.

Tests were conducted on a 1/75-scale model in the Langley Unitary Plan wind tunnel at Mach numbers of 1.60, 2.16, and 2.86, at angles of attack from approximately -4° to 26°, and generally at angles of sideslip of 0° and 4°. The Reynolds number per foot was held constant at 2.5×10^{6}.

SYMBOLS

Longitudinal force and moment coefficients were referred to the stability axes and the lateral and directional force and moment coefficients were referred to the body axes. The moment reference center was located at 15 percent of the mean aerodynamic chord of the first-stage wing and was 12.467 inches forward of the model base in the stage-separation plane. (See fig. 1(a).) All aerodynamic coefficients are based on the geometry of the wing of the first-stage reusable booster.

C_L lift coefficient, $\frac{\text{Lift}}{qS}$

$C_{L,(L/D)_{max}}$ lift coefficient at maximum lift-drag ratio

C_D drag coefficient, $\frac{\text{Drag}}{qS}$

$C_{D,o}$ drag coefficient at zero lift

C_m pitching-moment coefficient, $\frac{\text{Pitching moment}}{qS\bar{c}}$

$C_{m,o}$ pitching-moment coefficient at zero lift

C_l rolling-moment coefficient, $\frac{\text{Rolling moment}}{qSb}$

C_n yawing-moment coefficient, $\frac{\text{Yawing moment}}{qSb}$

C_Y side-force coefficient, $\frac{\text{Side force}}{qS}$

C_{L_α} lift-curve slope at zero lift, $\frac{\partial C_L}{\partial \alpha}$, per deg

$C_{m_{C_L}}$ longitudinal-stability parameter at zero lift, $\frac{\partial C_m}{\partial C_L}$

C_{m_δ} control effectiveness of canard, $\frac{\Delta C_m}{\Delta \delta}$, per deg

$\frac{\partial C_D}{\partial C_L{}^2}$ drag-due-to-lift parameter

C_{l_β} effective-dihedral parameter, $\frac{\Delta C_l}{\Delta \beta}$, per deg

C_{n_β} directional-stability parameter, $\frac{\Delta C_n}{\Delta \beta}$, per deg

C_{Y_β} side-force parameter, $\frac{\Delta C_Y}{\Delta \beta}$, per deg

b	reference wing span, 1.333 ft
c	local chord, ft
$\bar{c}$	reference mean aerodynamic chord, based on total wing area, 1.222 ft
L/D	lift-drag ratio, $\frac{C_L}{C_D}$
$(L/D)_{max}$	maximum lift-drag ratio
M	free-stream Mach number
q	free-stream dynamic pressure, lb/sq ft
S	reference wing area, 1.222 sq ft
α	angle of attack (referred to stage-separation plane), deg
β	angle of sideslip, deg
δ	angle of canard deflection (positive for leading edge up), deg

Component designations:

B	fuselage, first- or second-stage
W	wing, first- or second-stage
C	canard, $\delta = 0^\circ$
C'	canard, $\delta = -5^\circ$
N	nacelles, first-stage
F	vertical fins, first- or second-stage
M	maneuver propulsion package
S	spacecraft with mounting pad

DESCRIPTION OF MODEL

The complete launch vehicle and its components are shown in figure 1. The launch vehicle consisted of a winged reusable first stage with a canard, a winged reusable second stage, and a winged third-stage reusable spacecraft with an expendable space-maneuvering propulsion package. The two upper stages were

arranged in tandem, and this combination was placed parallel to the first-stage reusable booster. Principal model dimensions are presented in table I, and photographs of the model are shown in figure 2.

First-Stage Reusable Booster

The first-stage reusable booster consisted of a semicylindrical fuselage with an ogival forebody, a delta canard, and a delta wing with trapezoidal vertical fins mounted outboard on nacelles. (See fig. 1(b).) The wing had 70° of leading-edge sweep and was a symmetrical wedge to the 40-percent-chord station with a constant 0.05c maximum thickness rearward to the 0.85c station. A wedge or boattail on the lower surface of the wing extended from 0.85c to the wing trailing edge. (See fig. 1(c).) The first-stage wing was flat on the upper surface rearward of the 40-percent-chord station to allow mating with the second-stage wing. The wing was set at an incident angle of 0°. The requirement for a flat upper surface resulted in a wing dihedral angle of about $3\frac{1}{2}^{\circ}$. The exposed area of the canard was approximately 7 percent of the total first-stage wing area, and the distance between $0.25\bar{c}$ of the canard and $0.25\bar{c}$ of the first-stage wing was $1.4\bar{c}$ of the wing. Provision was made for testing the canard at incidence angles of 0° and -5°.

The first-stage vertical fins were located outboard at two-thirds of the wing semispan, and the total fin area, which was equally distributed above and below the wing, was approximately 15 percent of the total wing area. The vertical fins had a panel aspect ratio of 1.15 and a taper ratio of 0.5. The nacelles were cylindrical with a parabolic nose and were considered to house the flyback engines. The nacelles formed the juncture between the first-stage wing and vertical fins.

Second-Stage Reusable Booster

The second-stage reusable booster consisted of a cylindrical fuselage $7\frac{1}{2}$ diameters long (including an interstage of 1 diameter length to allow for the nose of the second-stage fuselage) and a trapezoidal wing with two outboard-mounted vertical fins located at two-thirds of the wing semispan. The fuselage incorporated a side fairing which extended vertically from the center line of the second-stage fuselage to the upper surface of the first-stage fuselage.

The second-stage wing thickness was chosen to achieve a total profile thickness of 0.065c (based on the chord of the first-stage wing) when the first- and second-stage wings were mated. The forward 0.40c of the upper surface of the second-stage wing formed a coplanar surface with the first-stage wing. A portion of the leading edge of this extension was removed to form a constant leading-edge radius on the second-stage wing identical to that of the first-stage wing. The purpose of this arrangement was to reduce the interference of the mated wings during launch. The second-stage vertical fins were similar to the first-stage vertical fins, but only the upper element was employed.

Orbital Stage

The orbital stage consisted of a spacecraft and a maneuver propulsion package. The spacecraft was a wing-body configuration with toed-in wing-tip-mounted vertical fins. (See fig. 1(d).) The spacecraft wing was unsymmetrical with the camber adjacent to the spacecraft pad, and the span (including vertical fins) was approximately equal to the width of the first-stage fuselage. The maneuver propulsion package was an expendable rocket booster designed as a short cylinder with the same diameter as the second-stage fuselage and also incorporated the same type of side fairing as the second-stage fuselage. When the model was tested without the maneuver propulsion package, the spacecraft was moved rearward to connect directly with the second-stage fuselage. This configuration was considered to meet some other mission requirement not needing appreciable in-orbit maneuvering.

APPARATUS AND TESTS

The tests were conducted in the Langley Unitary Plan wind tunnel at Mach numbers of 1.60, 2.16, and 2.86, angles of attack from approximately -4° to 26°, angles of sideslip generally of 0° and 4°, and a constant Reynolds number per foot of 2.5×10^6. The tunnel stagnation temperature was kept constant at 150° F.

Static aerodynamic force and moment data were obtained by means of a six-component internally mounted strain-gage balance. Boundary-layer transition was fixed on the model by the method described in reference 9 with a 1/16-inch-wide strip of No. 60 carborundum grains (0.0118 inch in diameter) located 1 inch rearward of the first-stage nose, 1/4 inch rearward of the leading edge of the wings, and 1/8 inch rearward of the leading edge of the vertical fins.

Angles of attack and sideslip were corrected for balance and sting deflection under load. The drag of the vehicle was corrected to correspond to a base pressure equal to the free-stream static pressure on the first-stage fuselage and that portion of the first-stage wing base intercepted by the fuselage, unless otherwise noted. No pressure corrections were applied to the base area of the second-stage reusable booster.

PRESENTATION OF RESULTS

The basic longitudinal aerodynamic characteristics of the first stage and the launch vehicle are shown in figures 3 and 4, respectively; some of these results are summarized in figures 5 and 6. The basic lateral aerodynamic characteristics of the first stage are shown in figure 7. In addition, the lateral- and directional-stability parameters for the first stage and the launch vehicle are shown in figures 8 and 9, respectively; some of these results are summarized in figure 10. In the data figures, the various components are identified by letter symbols for purposes of configuration identification. (See symbol list

for component designations.) An outline of the contents of the data figures is as follows:

	Figure
Longitudinal aerodynamic characteristics at $\beta = 0^\circ$ for:	
First stage with its several components and combinations	3
Launch vehicle with effect of maneuver propulsion package	4
Variation with Mach number at $\beta = 0^\circ$ of:	
Lift-curve slopes and longitudinal stability parameters for two first-stage configurations and complete launch vehicle	5
Drag-due-to-lift parameter, drag at zero lift, maximum lift-drag ratio, and lift coefficient at which maximum lift-drag ratio occurs for two first-stage configurations and complete launch vehicle	6
Variation with sideslip angle of rolling-moment, yawing-moment, and side-force coefficients at various angles of attack for complete first stage	7
Variation with angle of attack of lateral- and directional-stability parameters for:	
First stage with its several components and combinations	8
Launch vehicle with effect of maneuver propulsion package	9
Variation of lateral-directional-stability parameters with Mach number for two first-stage configurations and complete launch vehicle at $\alpha = 0^\circ$, 8°, and 16°	10

DISCUSSION

Except where noted the discussion will indicate the important aerodynamic characteristics of the complete first-stage reusable booster and the complete launch vehicle.

Longitudinal Aerodynamic Characteristics

First-stage reusable booster.- The lift-curve slope at zero lift for the complete first stage (fig. 5) decreased from about 0.033 to 0.024 as the Mach number was increased from 1.60 to 2.86. The decrease in C_{L_α} of 0.009 with Mach number is much less than the expected decrease of 0.030 indicated from flat-plate theory $\left(C_{L_\alpha} = \frac{4}{57.3\sqrt{M^2 - 1}}\right)$.

The first stage was longitudinally stable at zero lift about the selected moment reference center of $0.15\bar{c}$ at $M = 1.60$ and $M = 2.16$ but was only neutrally stable at $M = 2.86$. (See fig. 5.) The aerodynamic center on the first stage moved forward approximately $0.08\bar{c}$ as the test Mach number was increased from 1.60 to 2.86. Figure 3 shows that the complete first stage became unstable

at the higher lift coefficients at all Mach numbers. Removal of the canard produced expected improvements in longitudinal stability at $M = 1.60$ and 2.16, the only Mach numbers at which the complete effect of the canard was determined.

Figure 5 shows the control effectiveness of the canard on the first stage at $C_L = 0$ over the Mach number range of these tests. The data from the present investigation were extrapolated to data obtained in reference 7 at $M = 3.0$ since no control effectiveness data were obtained at $M = 2.86$. It is seen that C_{m_δ} decreased from about 0.0036 at $M = 1.60$ to an extrapolated value of 0.0026 at $M = 2.86$. Figures 3(a) and 3(b) show that the control effectiveness remained essentially constant throughout the lift range.

Drag at zero lift for the first stage (fig. 6) decreased from a value of 0.0275 to 0.0183 as the test Mach number was increased from 1.60 to 2.86. Since the actual return flight vehicle (BWCNF) would have the base drag included, addition of the base drag of the first-stage fuselage increased $C_{D,o}$ significantly at all Mach numbers. Maximum lift-drag ratios for the complete first stage remained nearly constant at 4.3 as the test Mach number was increased from 1.60 to 2.86. Including the base drag of the first-stage fuselage reduced $(L/D)_{max}$ values of the complete first stage about 18 percent at all Mach numbers.

Launch vehicle.- Figure 5 shows that the addition of the complete upper stages to the complete first stage had a negligible effect on C_{L_α} but caused a decrease in longitudinal stability at zero lift of about $0.08\bar{c}$ to $0.04\bar{c}$ throughout the test Mach number range. The complete launch vehicle had about $0.01\bar{c}$ static margin at $M = 1.60$ but was unstable at $M = 2.16$ and $M = 2.86$. Figures 4(a) and 4(b) show that removal of the maneuver propulsion package, accompanied by moving the spacecraft rearward on the vehicle, increased $C_{m_{C_L}}$ and $C_{m,o}$ at $M = 1.60$ but had a negligible effect at $M = 2.16$.

The addition of the complete upper stages to the complete first stage significantly increased $C_{D,o}$ at all test Mach numbers. (See fig. 6.) Since the launch vehicle would be rocket powered, the large increases in $C_{D,o}$ caused by adding the upper stages may not be too important. However, should these increases become important, better means of integrating the upper stages with the first stage should be investigated. The complete launch vehicle is shown to have a constant $(L/D)_{max}$ value of 3.20 as the test Mach number was increased from 1.60 to 2.86. (See fig. 6.) High L/D values in this supersonic speed range are necessary for increased range when the launch vehicle cannot continue its intended mission and must therefore perform a glide return toward the launch site or some selected abort landing site.

Lateral-Directional Aerodynamic Characteristics

First-stage reusable booster.- In figure 7 the rolling-moment coefficient and yawing-moment coefficient are essentially linear for the complete first stage between $\beta = \pm 4^\circ$, except at $M = 1.60$ and $\alpha = 23.5^\circ$, where C_l and

C_n are nonlinear. Figure 8 shows that the complete first stage had positive effective dihedral $\left(-C_{l_\beta}\right)$ throughout the positive angle-of-attack range and Mach number range of these tests. At angles of attack less than 10°, the complete first stage was directionally stable at $M = 1.60$ and 2.16 and was approximately neutrally stable at $M = 2.86$. At the higher angles of attack for $M = 1.60$ and $M = 2.16$ the canard had a significant favorable influence on both the effective dihedral and directional stability.

Launch vehicle.- The addition of the complete upper stages to the complete first stage caused a reduction in positive effective dihedral at all Mach numbers for angles of attack less than approximately 11°. (See fig. 9.) However, the launch vehicle had positive effective dihedral $\left(-C_{l_\beta}\right)$ throughout the positive angle-of-attack range and Mach number range of these tests. Figure 9 also shows that the addition of the complete upper stages to the complete first stage caused destabilizing increments in C_{n_β} at all Mach numbers. Removal of the maneuver propulsion package is seen to have a favorable influence on directional stability.

SUMMARY OF RESULTS

An investigation was made in the Langley Unitary Plan wind tunnel of a multistage horizontal-take-off reusable launch vehicle. The aerodynamic characteristics of the first-stage reusable booster and the launch vehicle with some stage and component effects were determined at Mach numbers of 1.60, 2.16, and 2.86, at angles of attack from approximately -4° to 26°, and generally at sideslip angles of 0° and 4°. The principal results may be summarized as follows:

1. For the selected moment reference center, the complete first stage was longitudinally stable at zero lift at Mach numbers of 1.60 and 2.16 but was only neutrally stable at a Mach number of 2.86; however, the complete first stage became unstable at the higher lift coefficients at all Mach numbers. The complete first stage also had positive effective dihedral throughout the positive angle-of-attack range and Mach number range of these tests. At angles of attack less than 10°, the complete first stage had at least neutral directional stability throughout the Mach number range.

2. The canard produced large reductions in longitudinal stability on the first stage but increased effective dihedral and directional stability significantly at high angles of attack.

3. Maximum lift-drag ratios for the complete first stage remained nearly constant at 4.3 throughout the test Mach number range. Including the fuselage base drag reduced maximum lift-drag ratios about 18 percent at all Mach numbers.

4. Addition of the complete upper stages to the complete first stage caused destabilizing increments both longitudinally and directionally, and caused reductions in positive effective dihedral at all test Mach numbers.

5. The complete launch vehicle was longitudinally stable at zero lift only at a Mach number of 1.60. The complete launch vehicle had positive effective dihedral throughout the positive angle-of-attack range and Mach number range but was directionally unstable at all Mach numbers.

6. Changing the upper-stage configuration significantly influenced both the longitudinal and directional stability of the complete launch vehicle.

Langley Research Center,
National Aeronautics and Space Administration,
Langley Station, Hampton, Va., January 21, 1965.

REFERENCES

1. Pierpont, P. Kenneth: Transonic Stability of a Preliminary Vertical-Take-Off Launch Configuration With a Horizontal-Landing Recoverable Booster. NASA TM X-689, 1962.

2. Pierpont, P. Kenneth: Transonic Longitudinal and Lateral Aerodynamic Characteristics of a Preliminary Concept of a First-Stage Horizontal-Take-Off-and-Horizontal-Landing Recoverable Booster With a 70° Delta Wing. NASA TM X-691, 1962.

3. Pierpont, P. Kenneth: Transonic Aerodynamic Characteristics of a Horizontal-Take-Off-and-Horizontal-Landing Recoverable-Booster Concept With Upper Stages Arranged in Parallel. NASA TM X-696, 1962.

4. Clark, Larry R.; and Pierpont, P. Kenneth: Hypersonic Aerodynamic Characteristics of Preliminary Vertical-Take-Off Launch Configurations With a Horizontal-Landing Reusable Booster. NASA TM X-887, 1963.

5. Clark, Larry R.; and Pierpont, P. Kenneth: Spacecraft and Stage-Geometry Effects on the Hypersonic Characteristics of a Horizontal-Take-Off Reusable Booster. NASA TM X-900, 1963.

6. Clark, Larry R.; and Pierpont, P. Kenneth: Transonic Characteristics of a Hydrogen-Fueled Multistage Horizontal-Take-Off Reusable Launch Vehicle. NASA TM X-1008, 1964.

7. Clark, Larry R.; and Decker, John P.: Longitudinal Aerodynamic Characteristics of a Model of a Horizontal-Take-Off Reusable Launch Vehicle at Mach Numbers From 3 to 6. NASA TM X-1030, 1964.

8. Decker, John P.; and Pierpont, P. Kenneth: Aerodynamic Separation Characteristics of Conceptual Parallel-Staged Reusable Launch Vehicle at Mach 3 to 6. NASA TM X-1051, 1965.

9. Braslow, Albert L.; and Knox, Eugene C.: Simplified Method for Determination of Critical Height of Distributed Roughness Particles for Boundary-Layer Transition at Mach Numbers From 0 to 5. NACA TN 4363, 1958.

TABLE I.- GEOMETRIC DESIGN CHARACTERISTICS OF THE MODEL

First Stage:	
Fuselage:	
Length, in.	39.600
Maximum diameter, in.	4.206
Maximum height, in.	3.203
Nose radius, in.	0.160
Base area, sq in.	11.567
Wing:	
Total area, sq in.	176
Exposed area, sq in.	95.700
Span, in.	16
Root chord, in.	22
Tip chord, in.	0
Maximum thickness, percent chord	5
Leading-edge sweep angle, deg	70
Leading-edge radius, in.	0.040
Mean aerodynamic chord, in.	14.667
Moment reference center, percent M.A.C.	15
Moment reference center, in. from base	12.467
Vertical fins:	
Area of each fin (exposed), sq in.	6.400
Height (exposed), in.	1.920
Root chord, in.	4.440
Tip chord, in.	2.220
Leading-edge sweep angle, deg	60
Trailing-edge sweep angle, deg	29.921
Leading-edge radius, in.	0.040
Wing nacelles:	
Length, in.	6.637
Maximum diameter, in.	0.960
Fineness ratio	6.914
Nose radius, in.	0.160
Canard:	
Total area, sq in.	35.568
Exposed area, sq in.	12.440
Span, in.	7.200
Root chord, in.	9.880
Tip chord, in.	0
Maximum thickness, percent chord	5
Leading-edge sweep angle, deg	70
Leading-edge radius, in.	0.040
Second Stage:	
Fuselage:	
Length, in.	16.000
Diameter, in.	2.134
Base area, sq in.	4.067
Wing:	
Total area, sq in.	75.200
Exposed area, sq in.	51.700
Span, in.	9.600
Root chord, in.	11.780
Tip chord, in.	3.852
Maximum thickness, percent chord	2.800
Leading-edge sweep angle, deg	58.75
Leading-edge radius, in.	0.040
Vertical fins:	
Area of each fin (exposed), sq in.	6.321
Height, in.	2.082
Root chord, in.	4.300
Tip chord, in.	2.220
Leading-edge sweep angle, deg	60
Trailing-edge sweep angle, deg	29.921
Leading-edge radius, in.	0.040

TABLE I.- GEOMETRIC DESIGN CHARACTERISTICS OF THE MODEL - Concluded

Orbital Stage:	
Fuselage:	
Length, including interstage, in.	10.080
Diameter, in.	1.120
Interstage base diameter, in.	2.134
Interstage taper, included angle, deg	35.2
Length of nose cone, in.	1.428
Nose cone included angle, deg	35
Nose radius, in.	0.160
Wing:	
Total area, sq in.	23.685
Exposed area (top surface), sq in.	14.852
Exposed area (bottom surface), sq in.	8.510
Span, in.	4.177
Root chord, in.	8.827
Tip chord, in.	2.648
Maximum thickness, percent chord	5
Leading-edge sweep angle, deg	72.5
Leading-edge radius, in.	0.040
Wing nose radius, in.	0.160
Vertical fins:	
Area, sq in.	2.405
Height, in.	1.430
Root chord, in.	2.648
Tip chord, in.	0.800
Maximum thickness, percent chord	5
Leading-edge sweep angle, deg	55
Leading-edge radius, in.	0.048
Lateral inclination angle, deg	3
Pad:	
Length, in.	10.080
Maximum width, in.	2.134
Nose radius, in.	0.160
Wedge included angle, deg	72.5
Maneuver-propulsion package:	
Length, in.	4.800
Diameter, in.	2.134

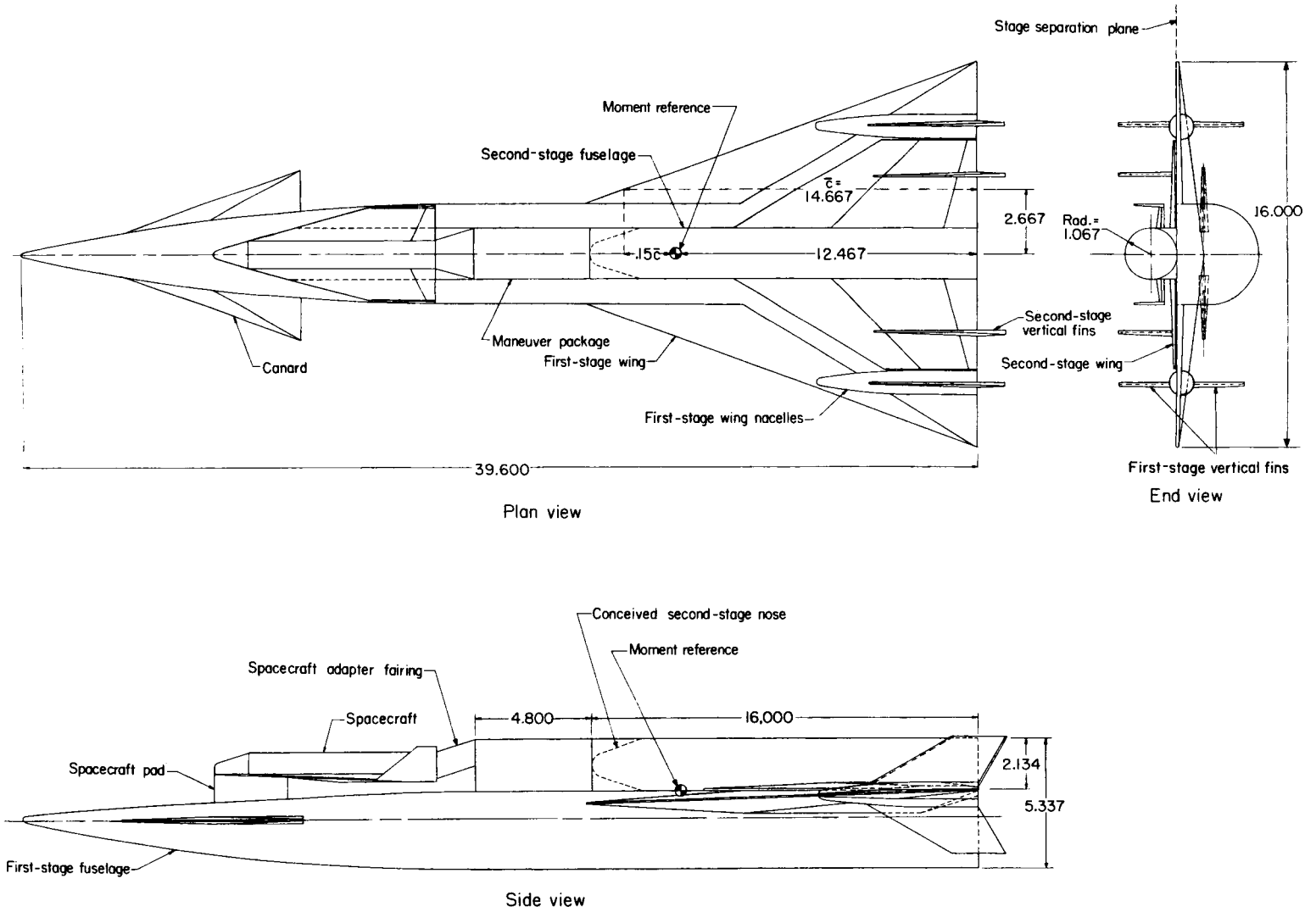

(a) General arrangement of the launch vehicle.

Figure 1.- Arrangement and geometric details of a three-stage horizontal take-off reusable booster system. All linear design dimensions are in inches.

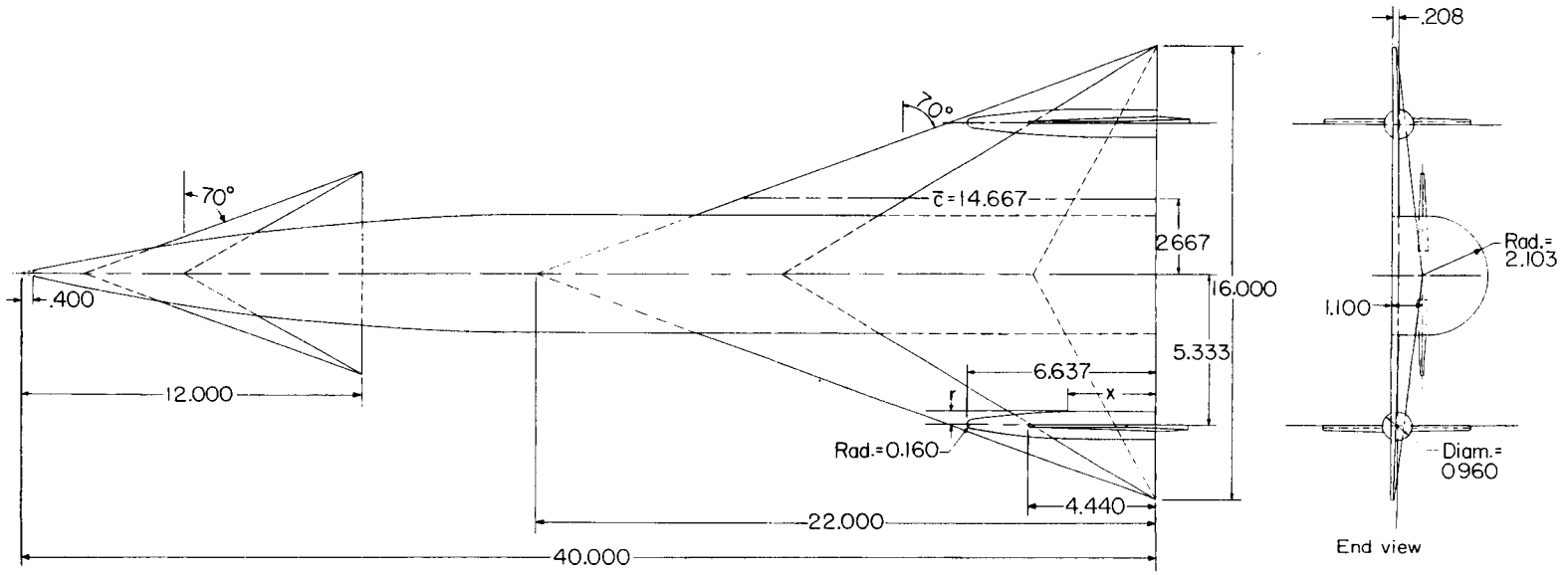

Wing-nacelle coordinates	
x	r
0	0 480
2 870	480
3 703	463
4 537	412
5.370	.327

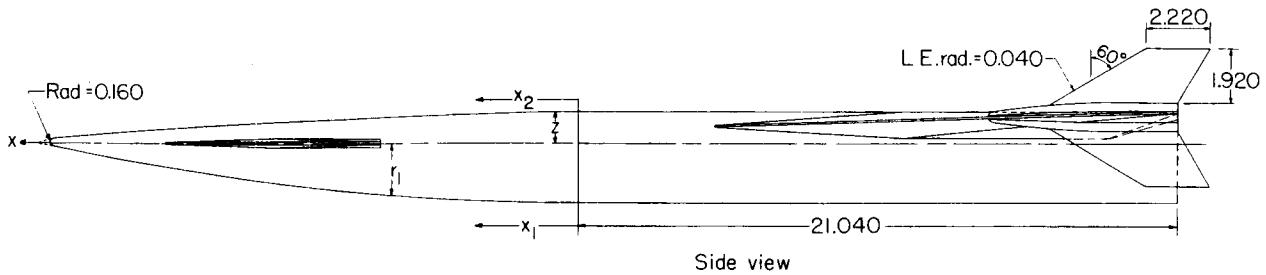

Fuselage coordinates			
x_1	r_1	x_2	z
0	2 103	0	1 100
1 667	2088	2 293	1 030
3 333	2038	3 960	978
5 000	1957	5 627	922
6 667	1 843	7 293	862
8 334	1697	8 960	798
10000	1517	10627	730
11 667	1 305	12 294	652
13 334	1 060	13 960	563
15 000	783	15 627	462
16 667	473	16 460	398
18 334	132	17 294	325
18960	0	17710	282
		18127	230
		18544	163
		18.960	0

(b) First-stage reusable booster.

Figure 1.- Continued.

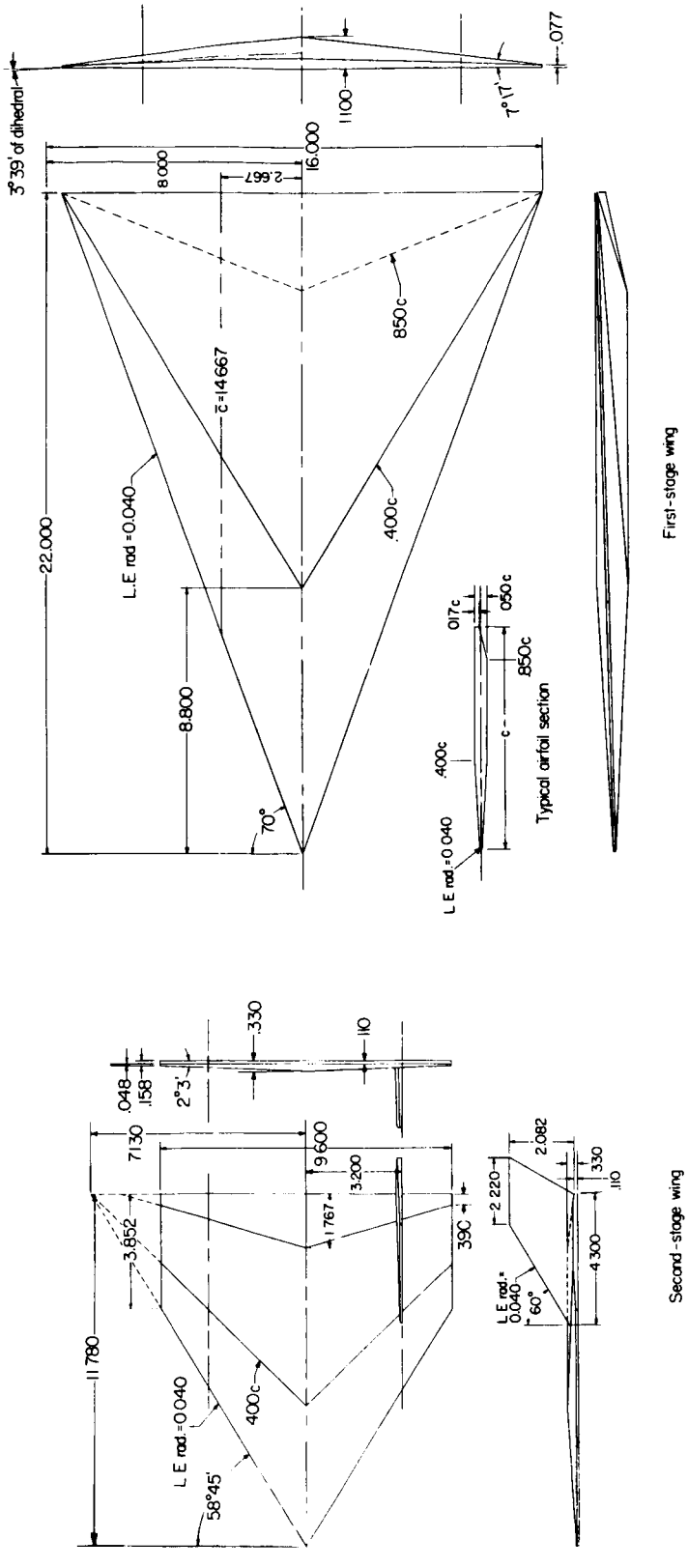

(c) Details of component parts.

Figure 1.- Continued.

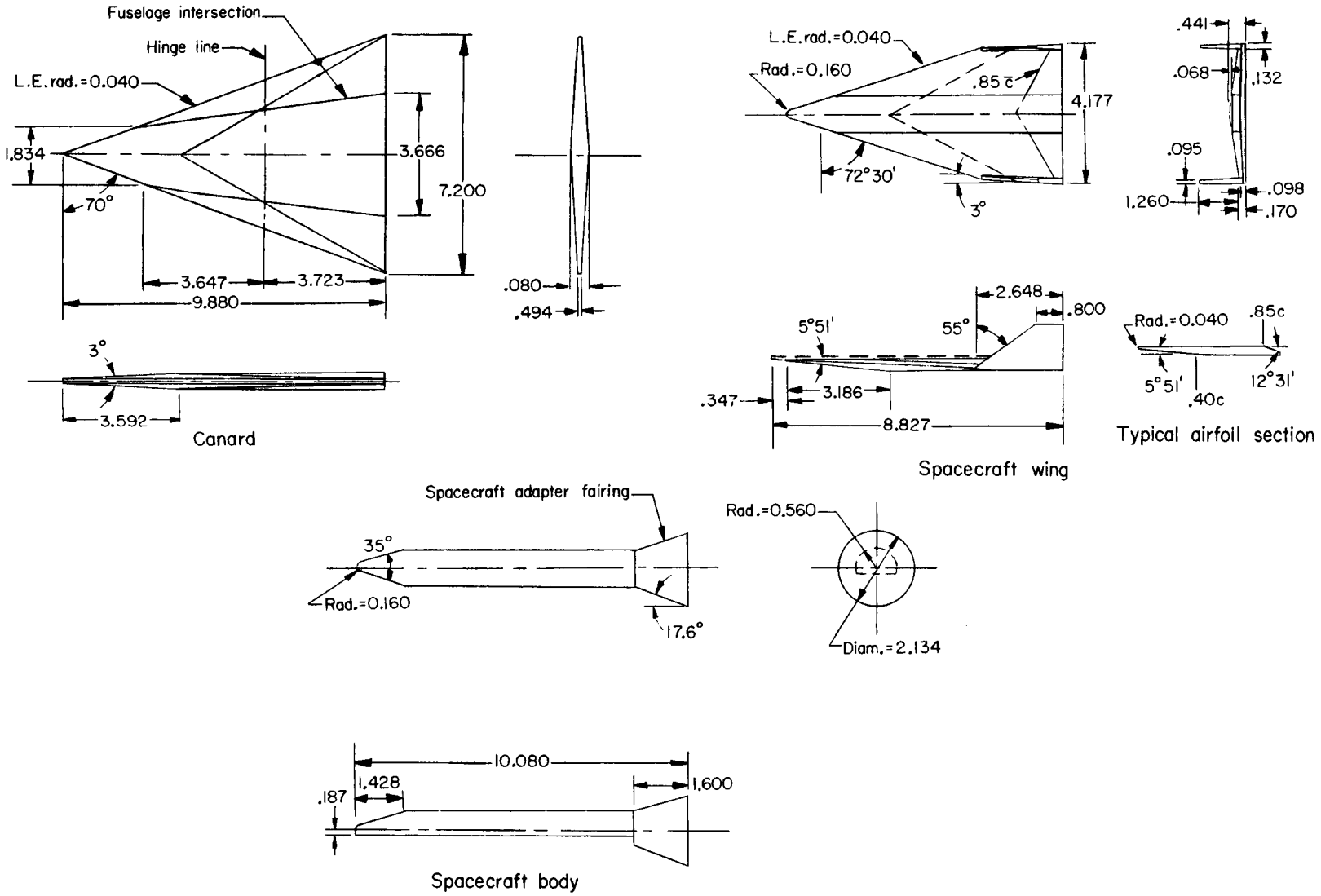

(d) Details of component parts.

Figure 1.- Concluded.

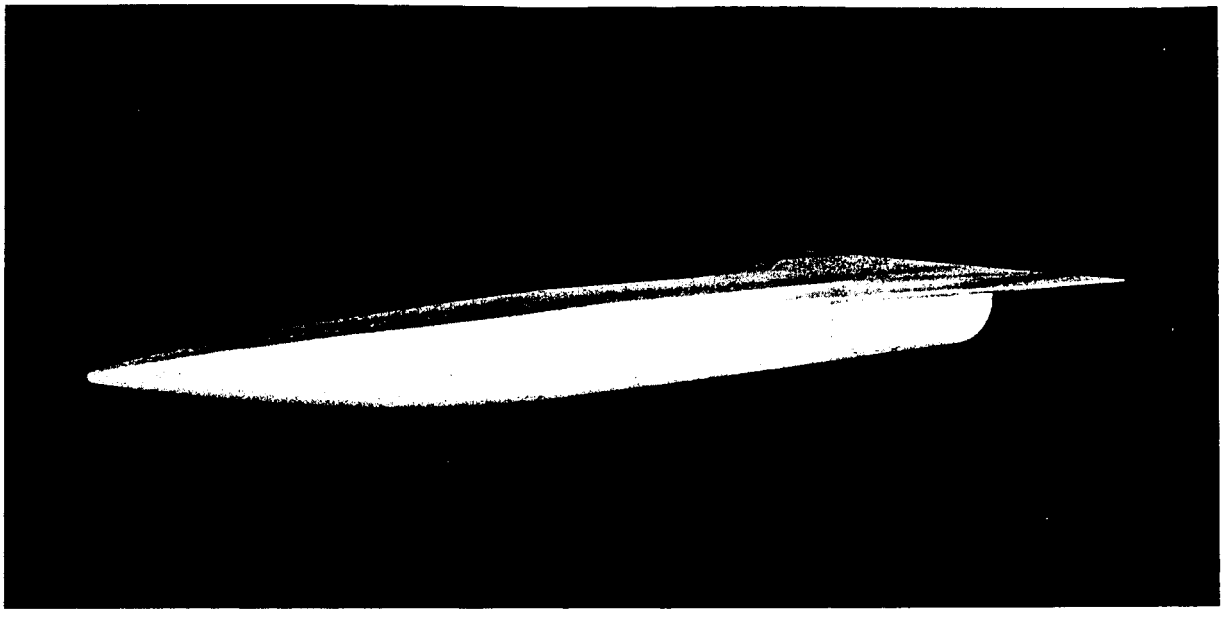

(a) First-stage wing-fuselage combination. L-63-6494

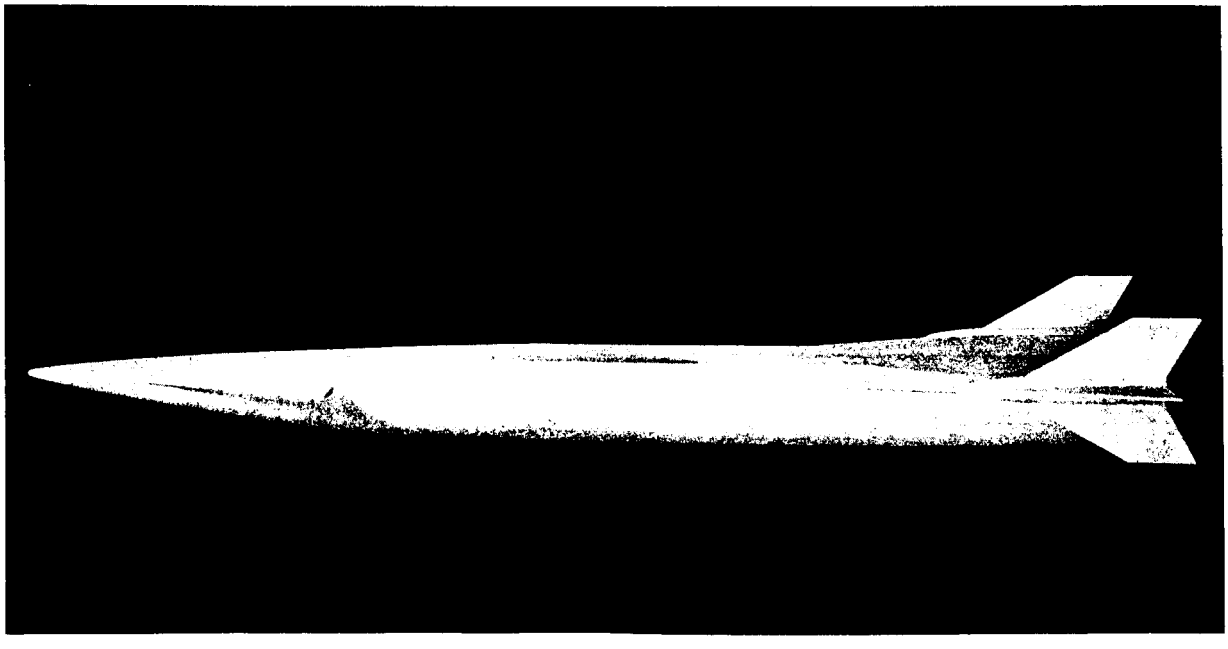

(b) Complete first-stage reusable booster. L-63-6483

Figure 2.- Photographs of model configurations.

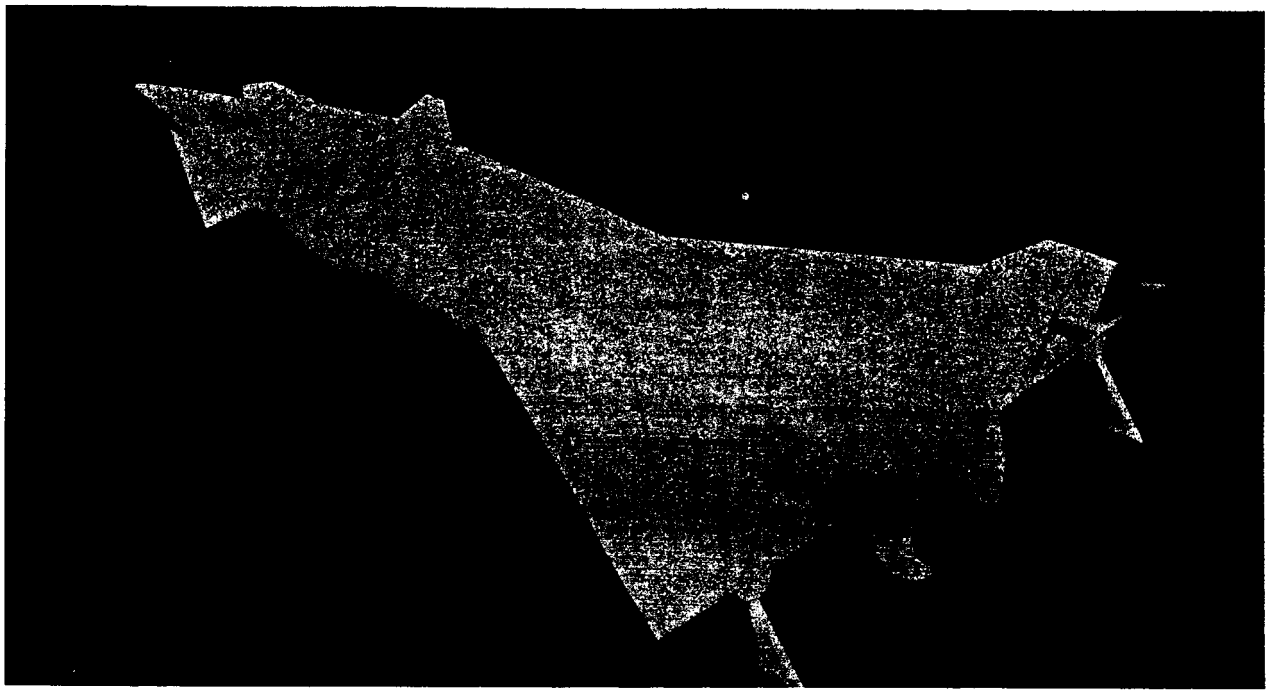

(c) Complete launch vehicle. L-63-6489

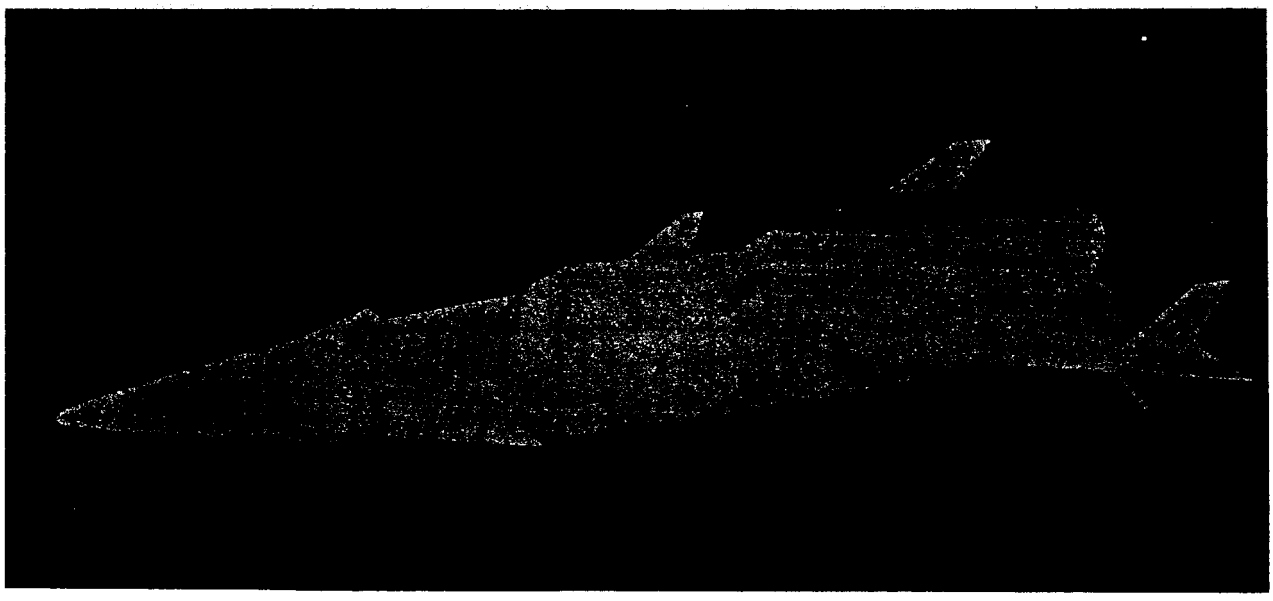

L-63-6481
(d) Launch vehicle without maneuver propulsion package.

Figure 2.- Concluded.

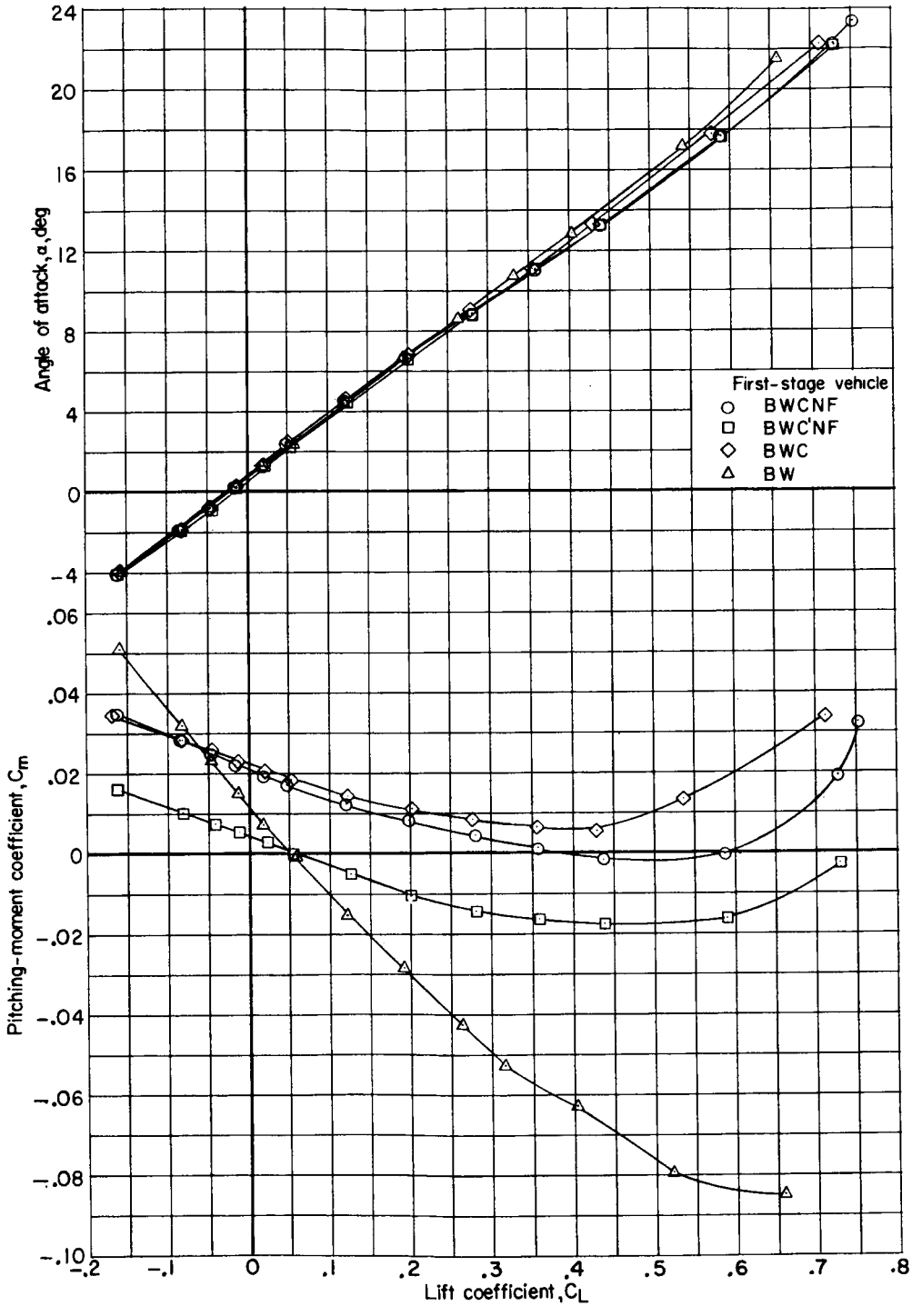

(a) M = 1.60.

Figure 3.- Longitudinal aerodynamic characteristics for several first-stage configurations. $\beta = 0^{\circ}$.

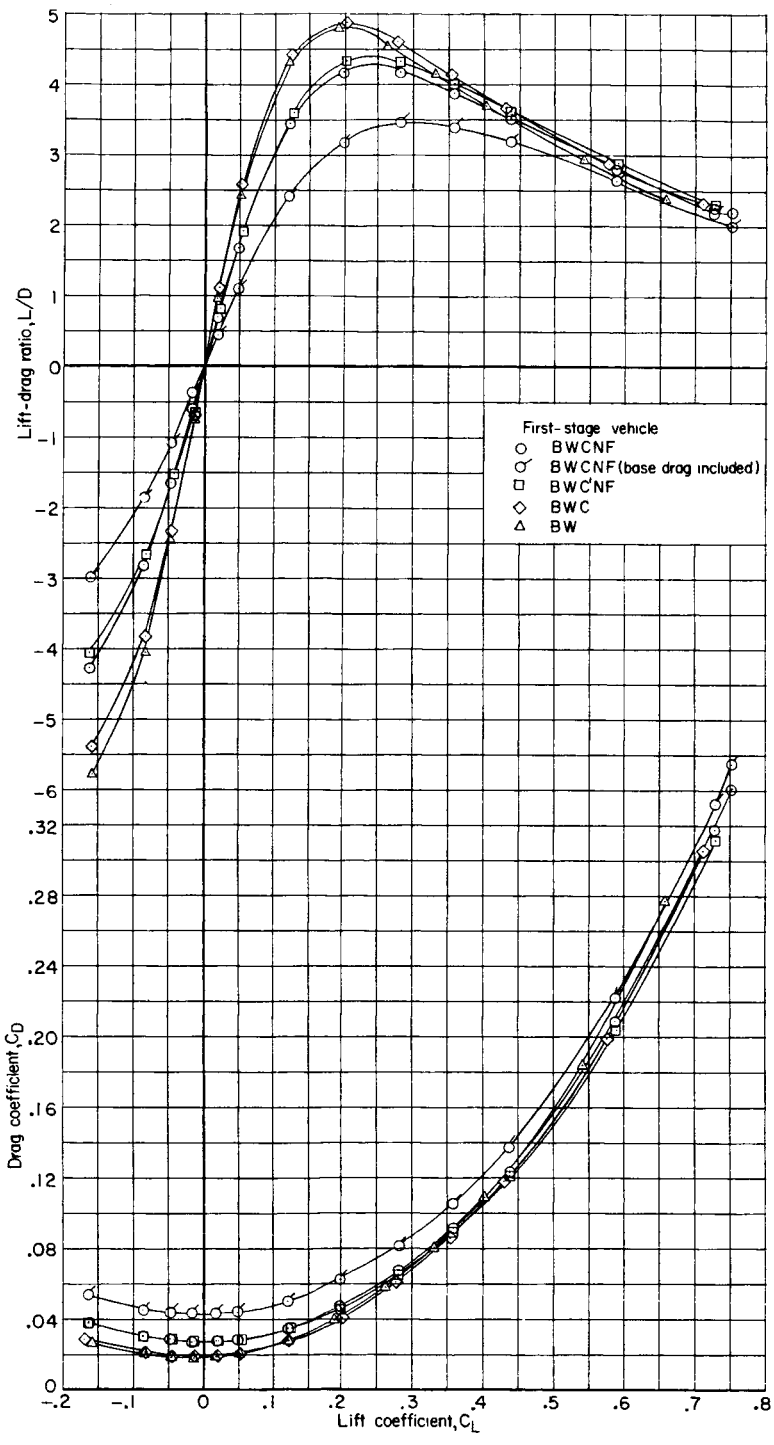

(a) M = 1.60 - Concluded.

Figure 3.- Continued.

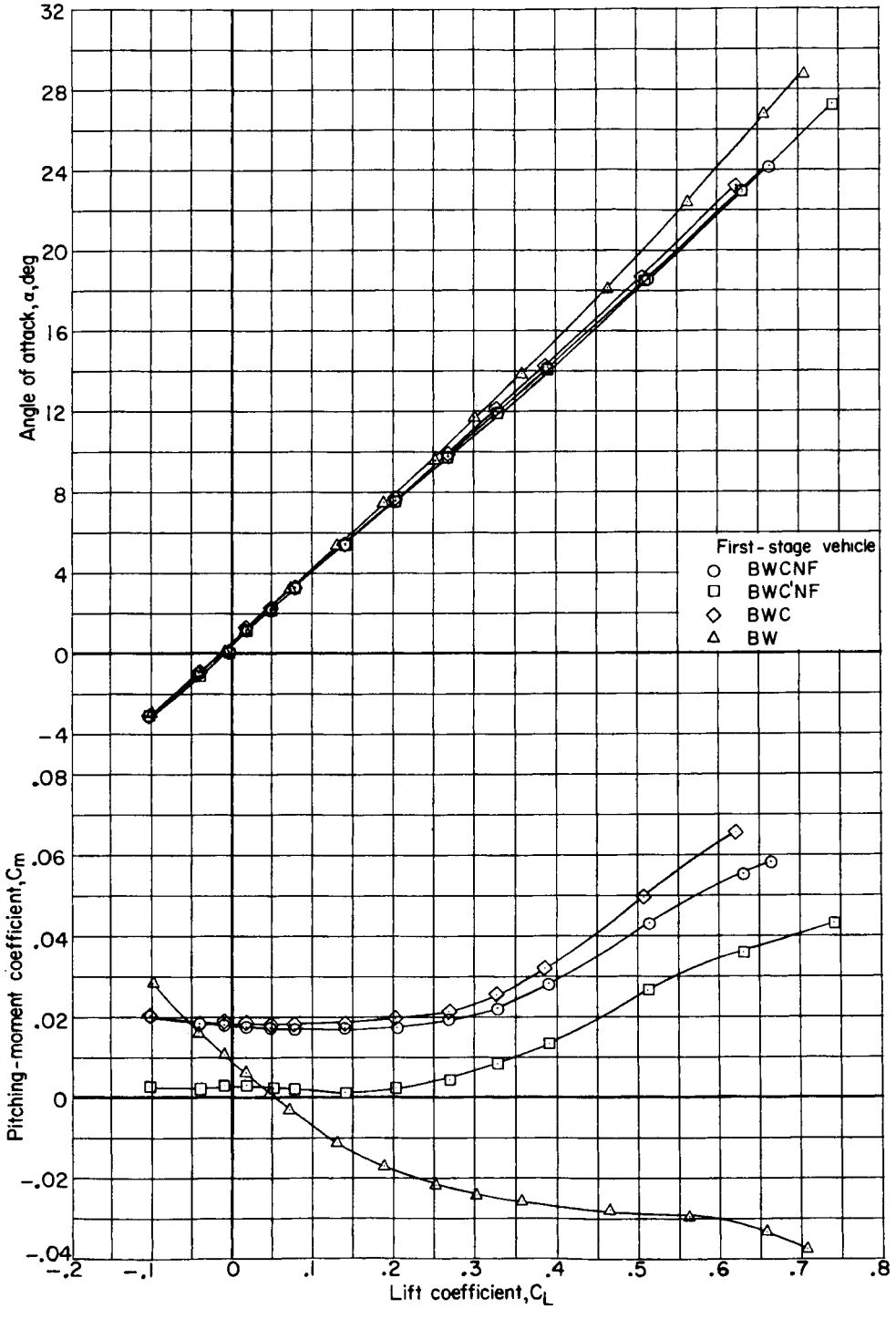

(b) M = 2.16.

Figure 3.- Continued.

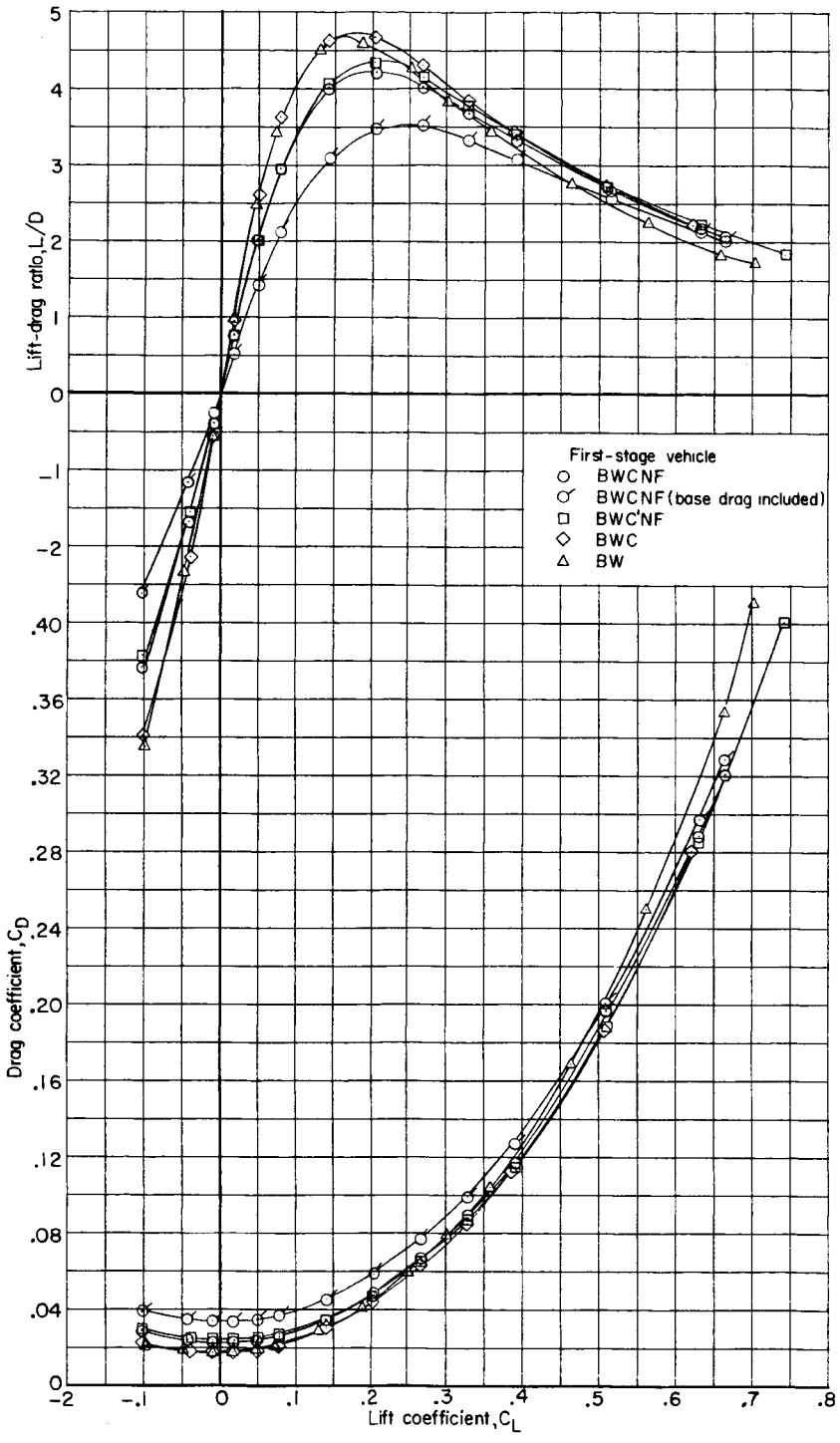

(b) M = 2.16 - Concluded.

Figure 3.- Continued.

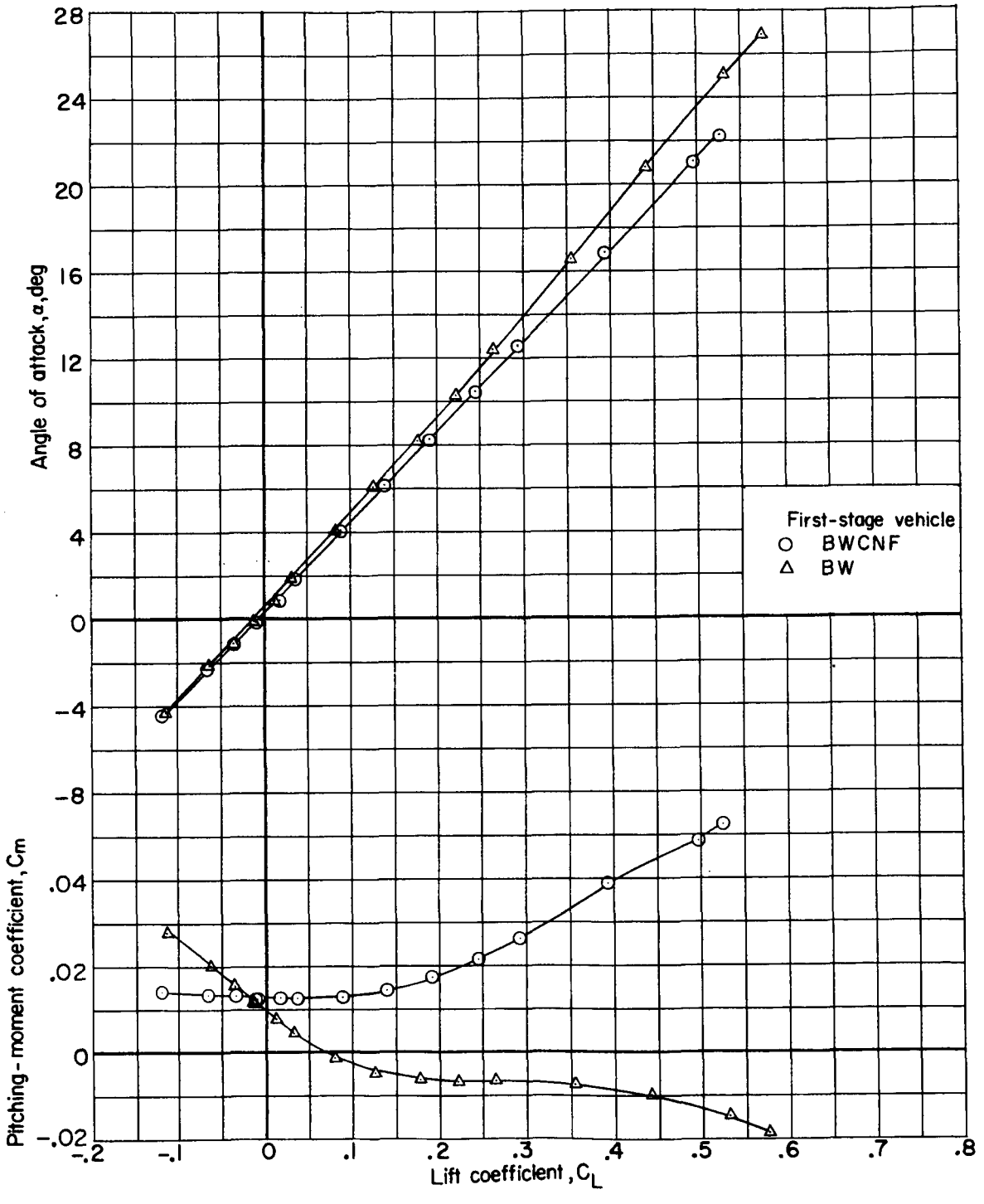

(c) M = 2.86.

Figure 3.- Continued.

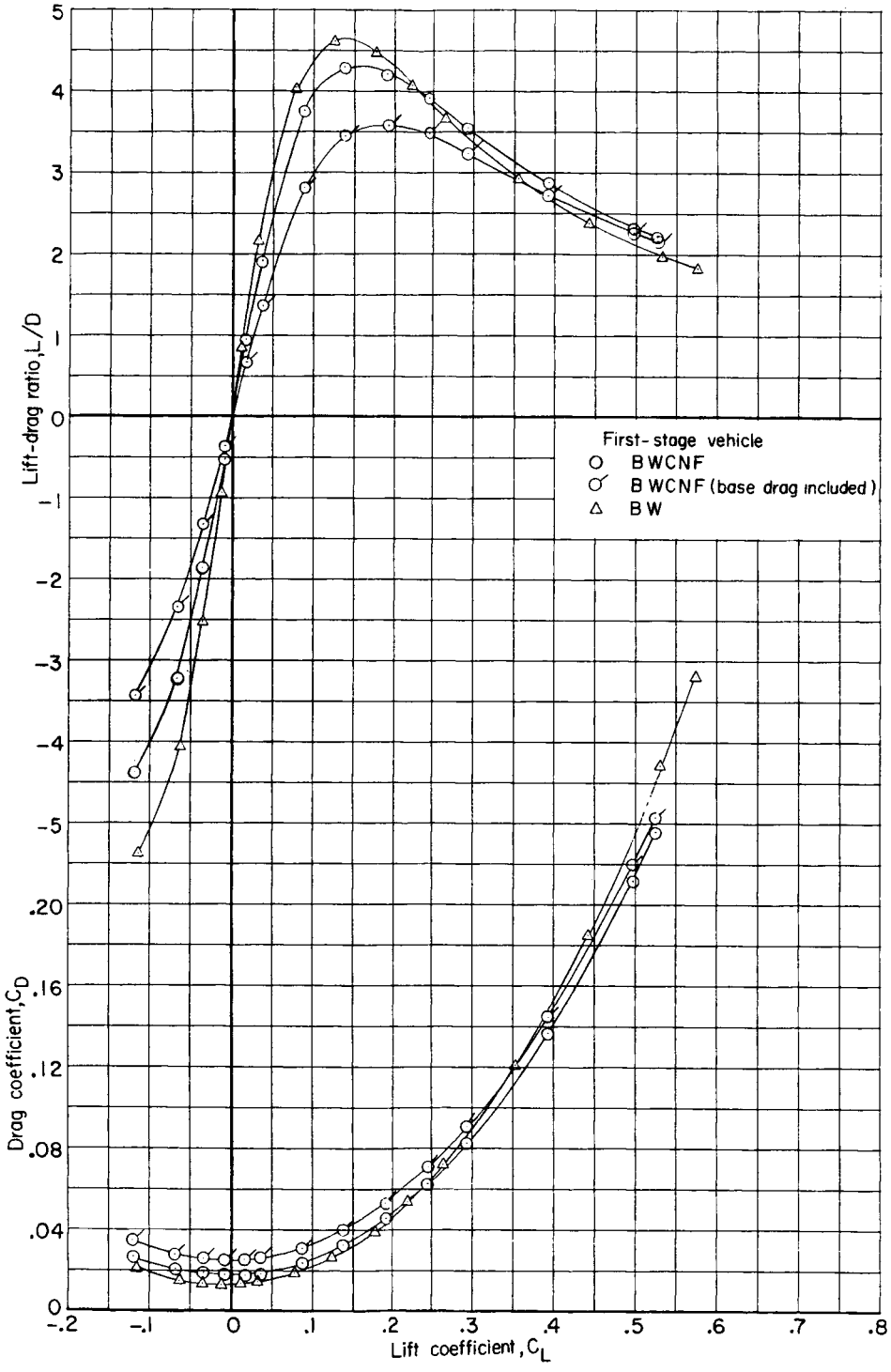

(c) M = 2.86 - Concluded.

Figure 3.- Concluded.

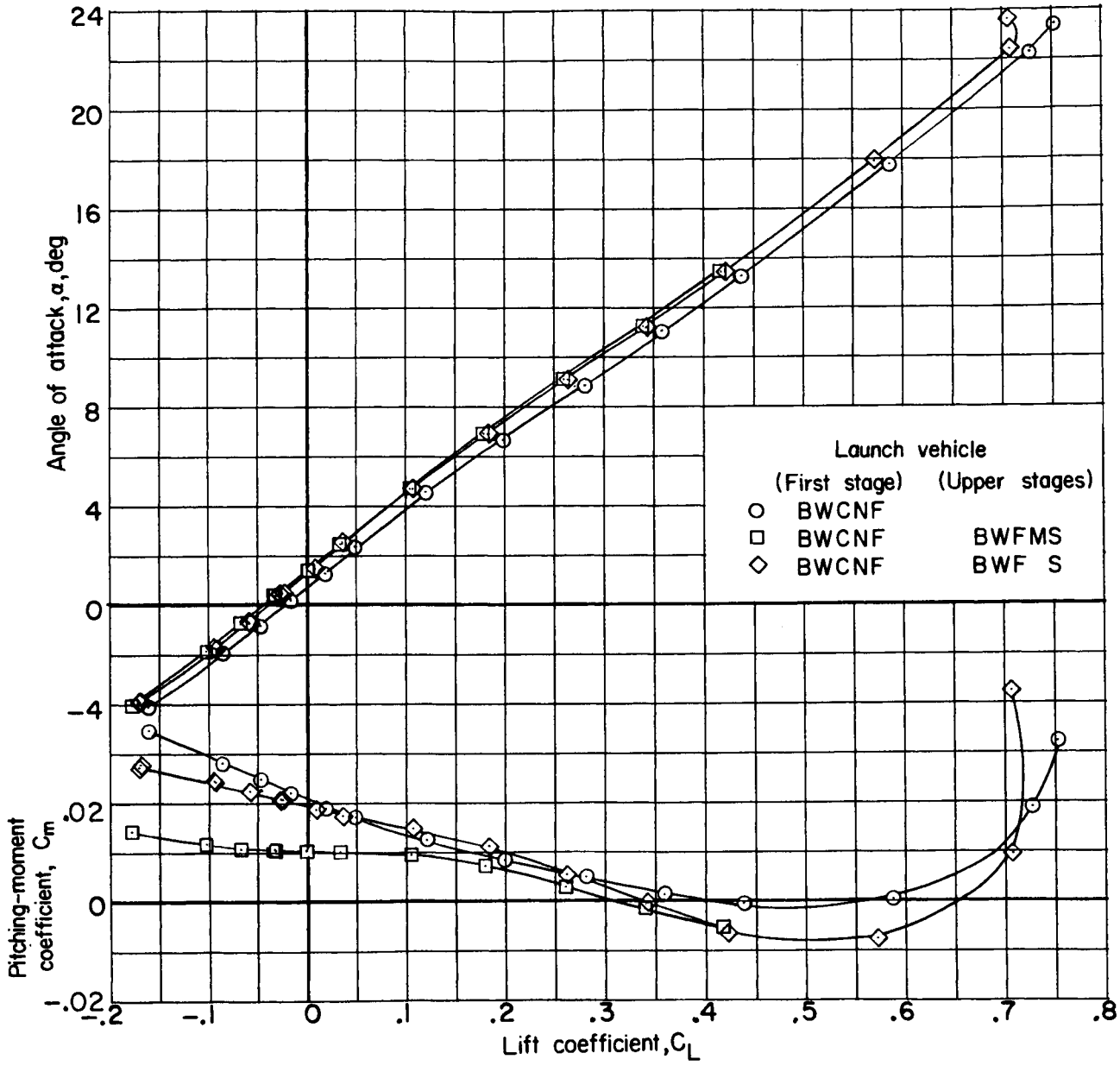

(a) M = 1.60.

Figure 4.- Longitudinal aerodynamic characteristics for the complete launch vehicle with the effect of the maneuver propulsion package.

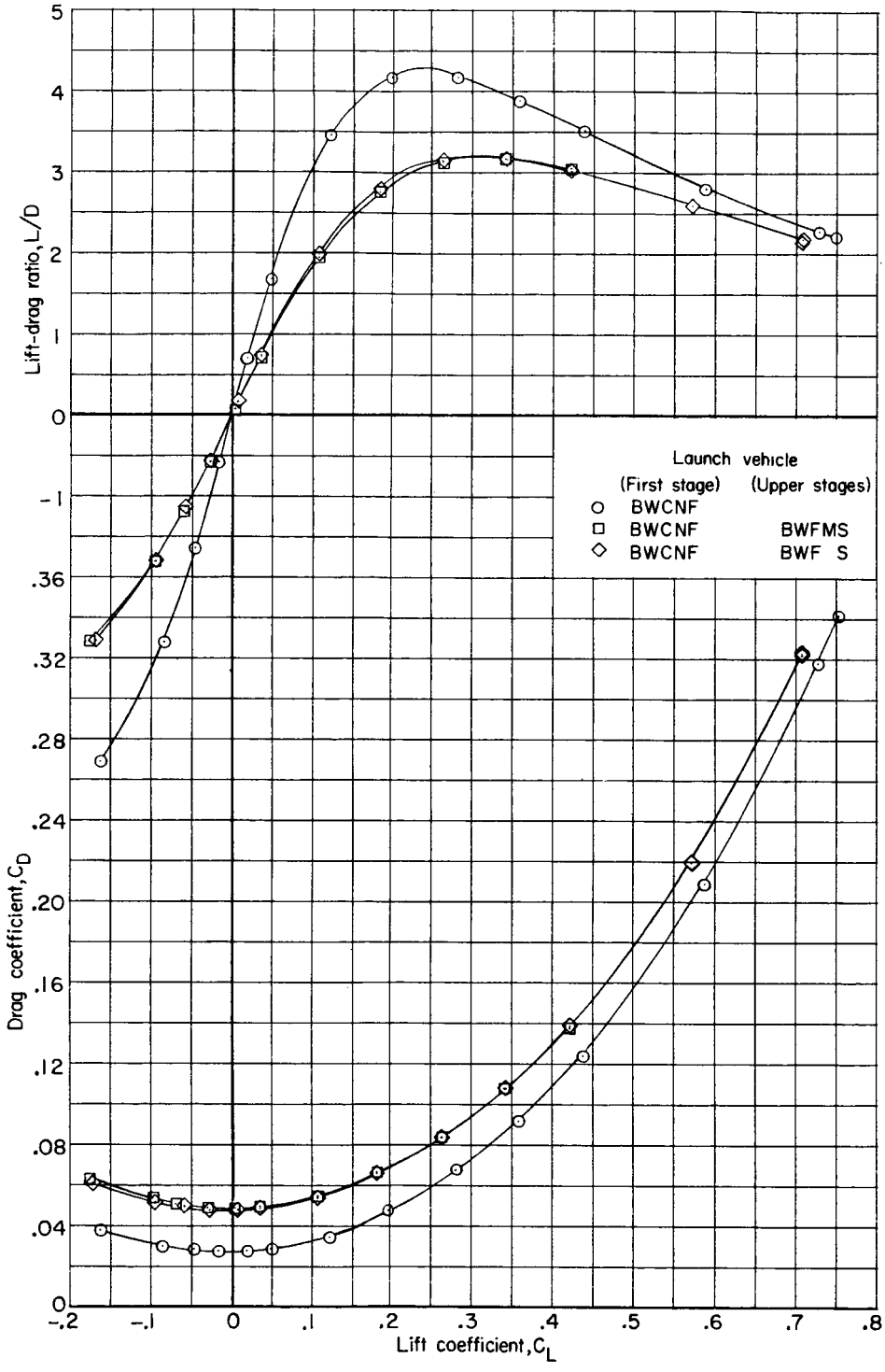

(a) M = 1.60 - Concluded.

Figure 4.- Continued.

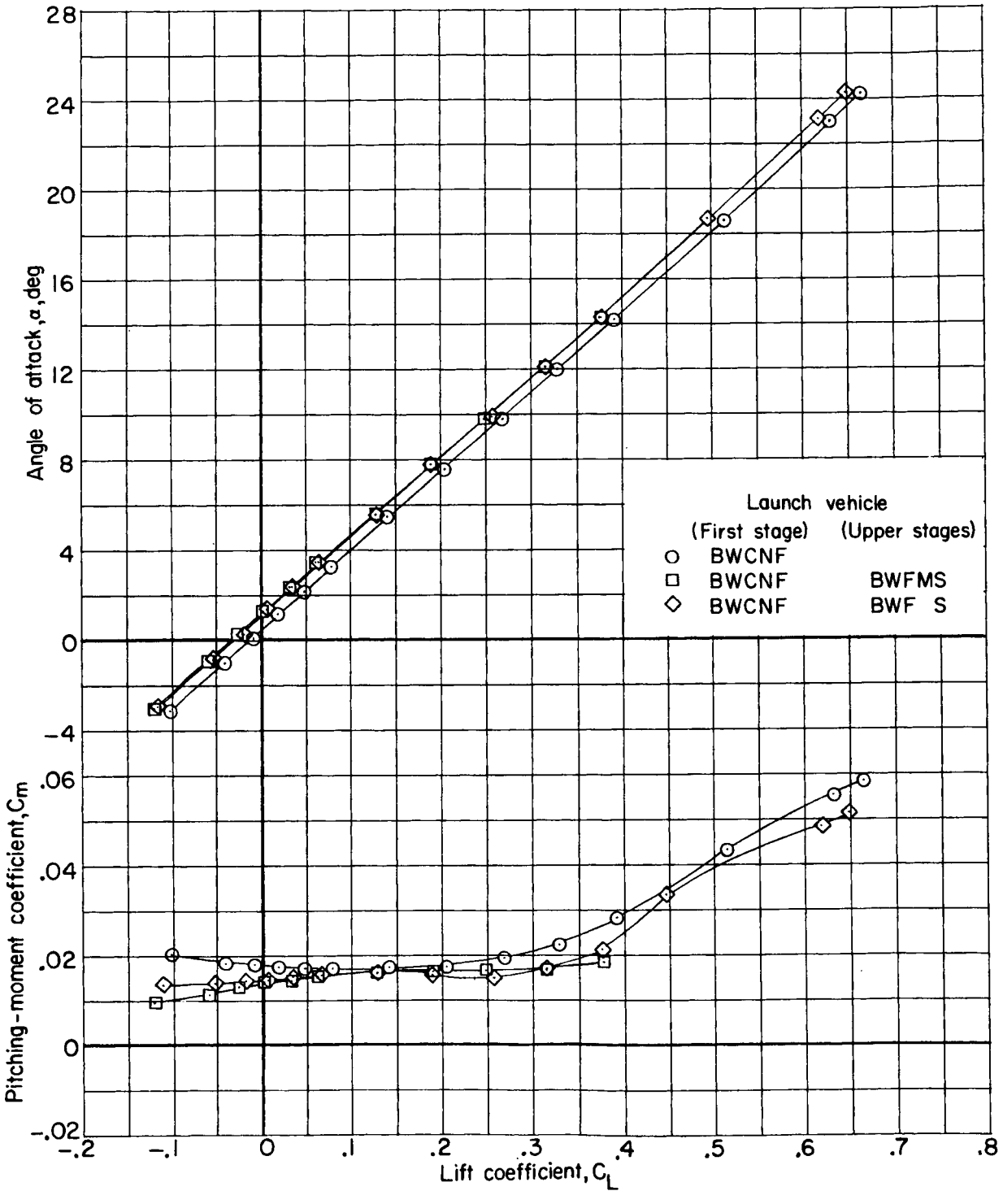

(b) M = 2.16.

Figure 4.- Continued.

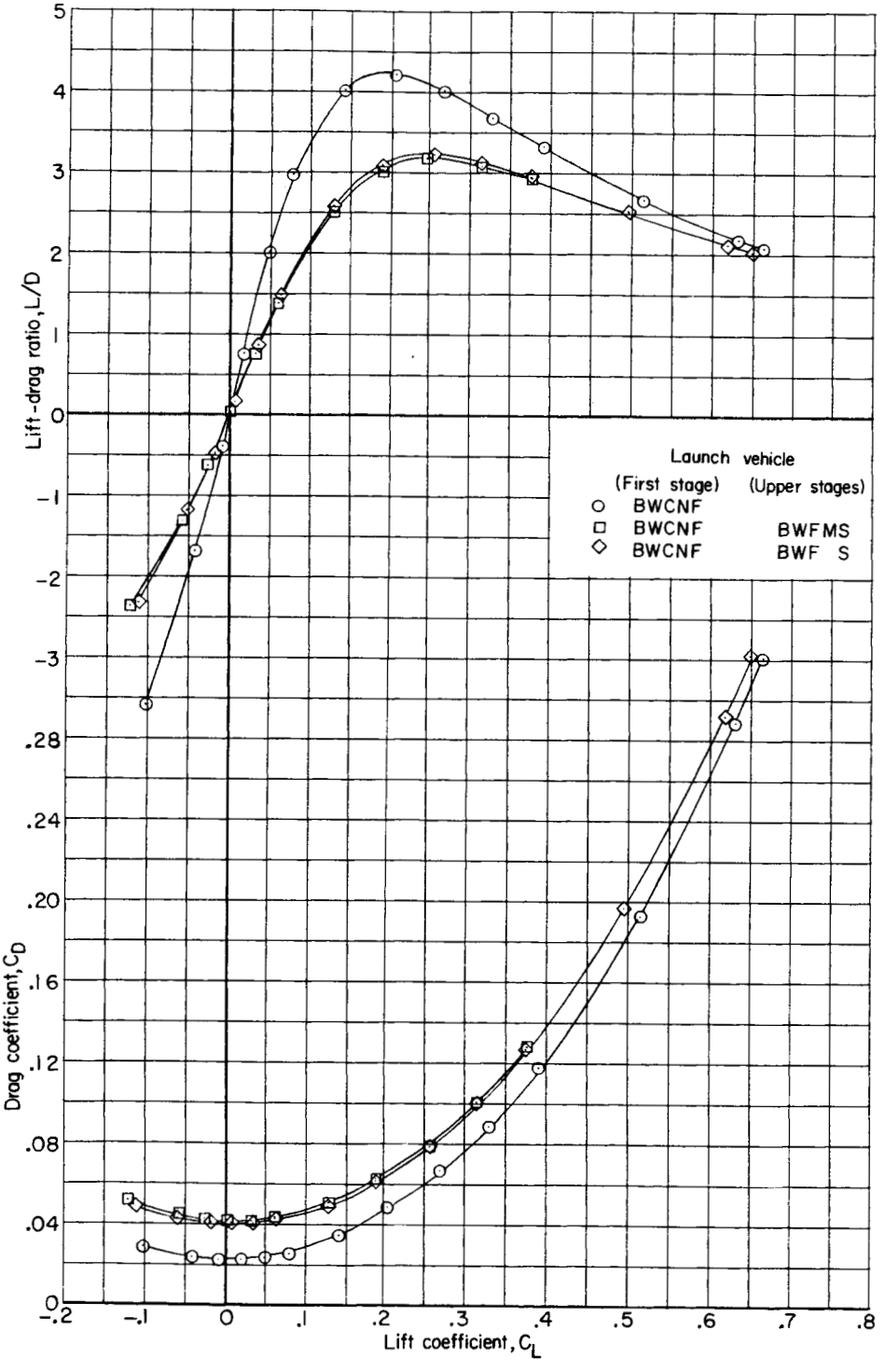

(b) M = 2.16 - Concluded.

Figure 4.- Continued.

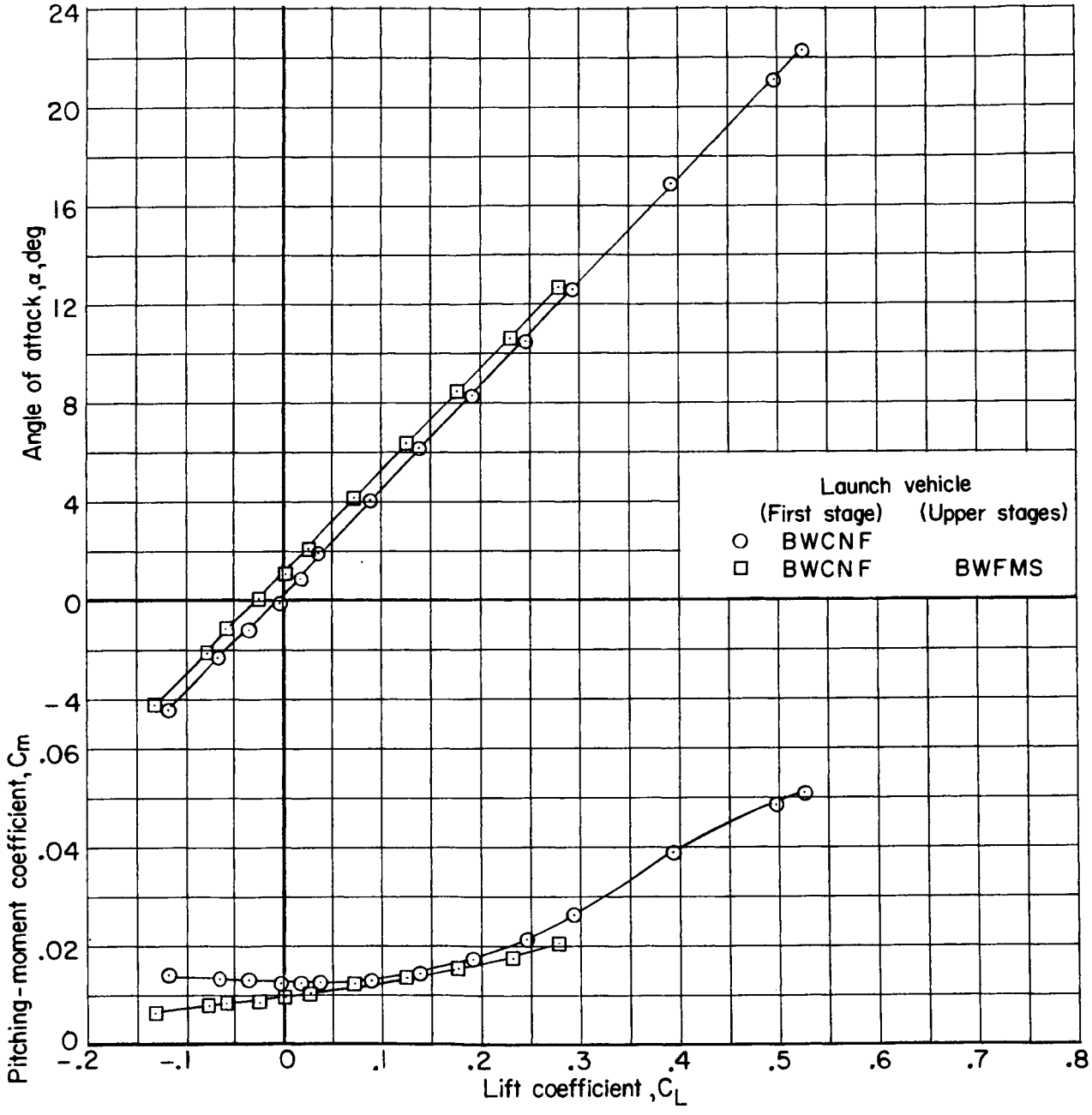

(c) M = 2.86.

Figure 4.- Continued.

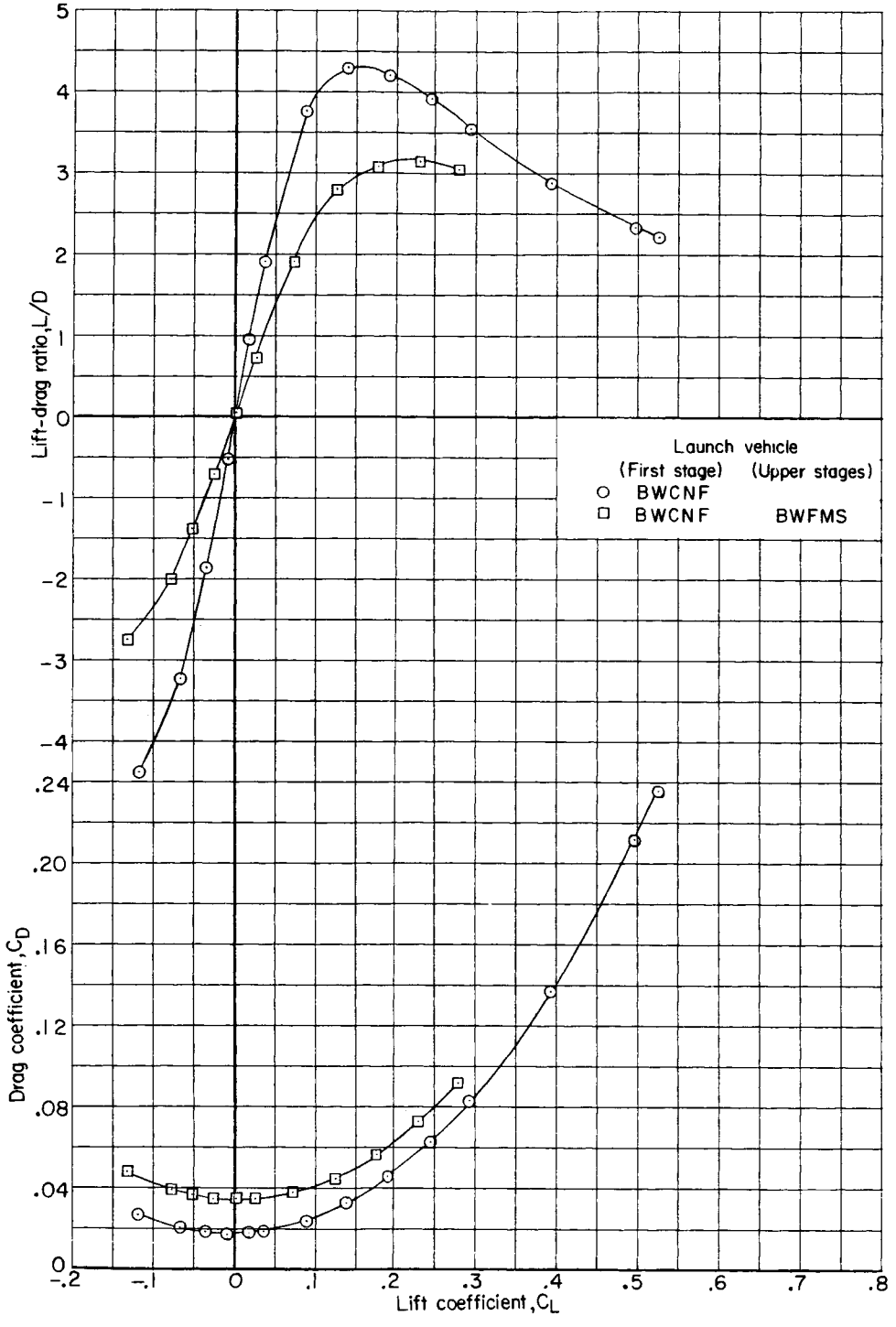

(c) M = 2.86 - Concluded.

Figure 4.- Concluded.

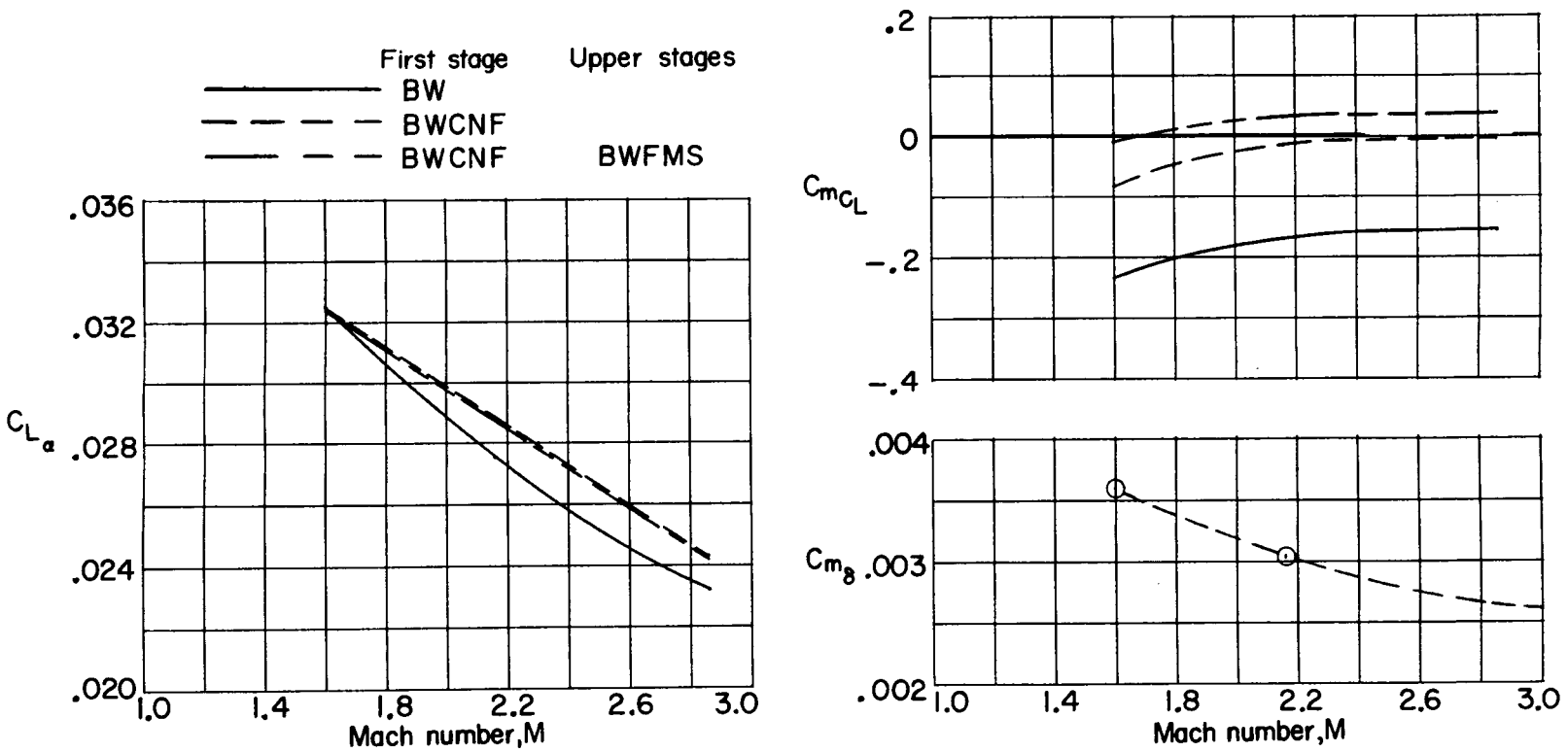

Figure 5.- Variation with Mach number of the lift-curve slopes and longitudinal stability parameters for two first-stage configurations and the complete launch vehicle. $\beta = 0^\circ$.

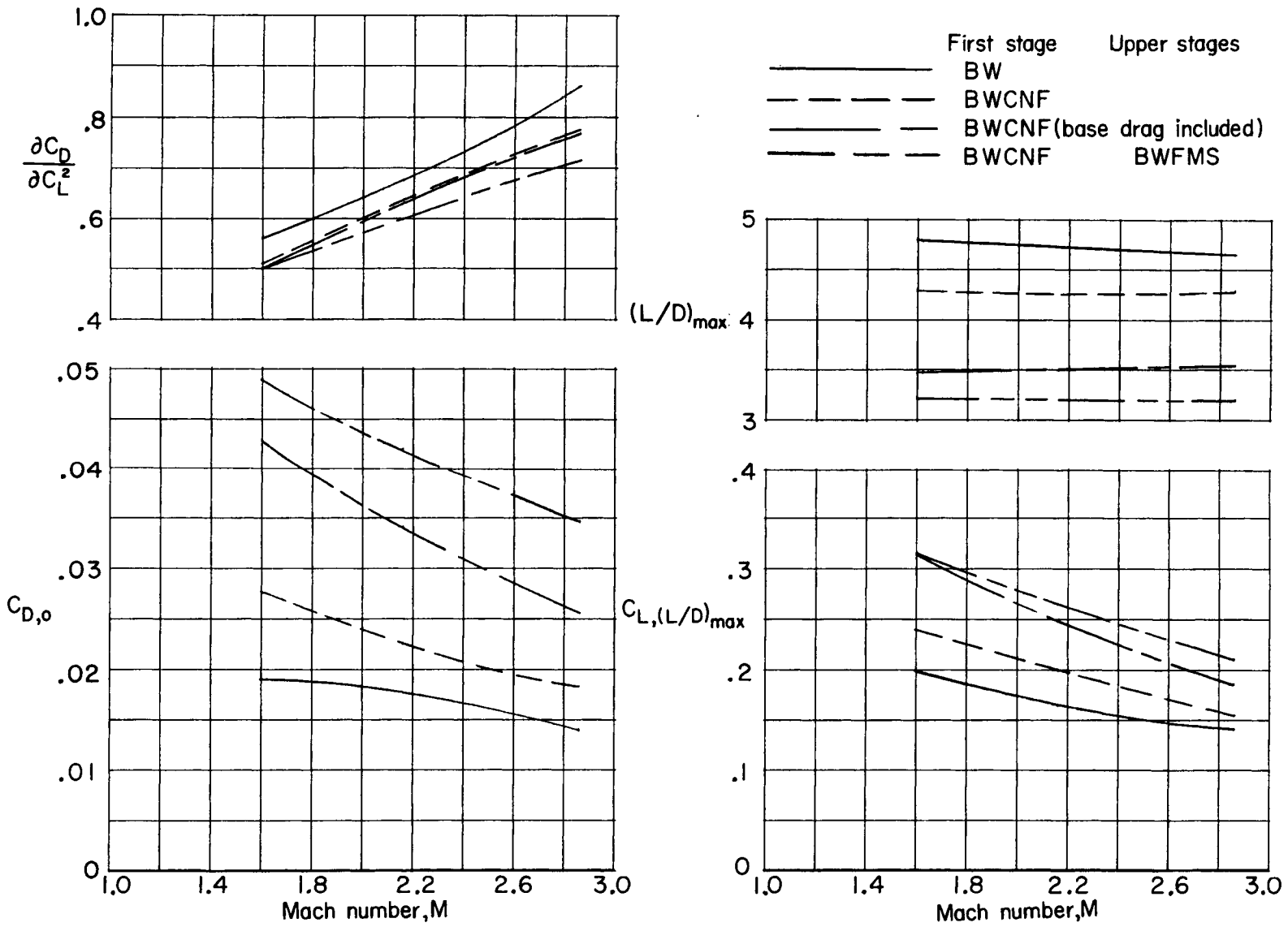

Figure 6.- Variation with Mach number of the drag due to lift, drag-at-zero-lift parameter, maximum lift-drag ratio, and the lift coefficient at which maximum lift-drag ratio occurs for two first-stage configurations and the complete launch vehicle. $\beta = 0^{o}$.

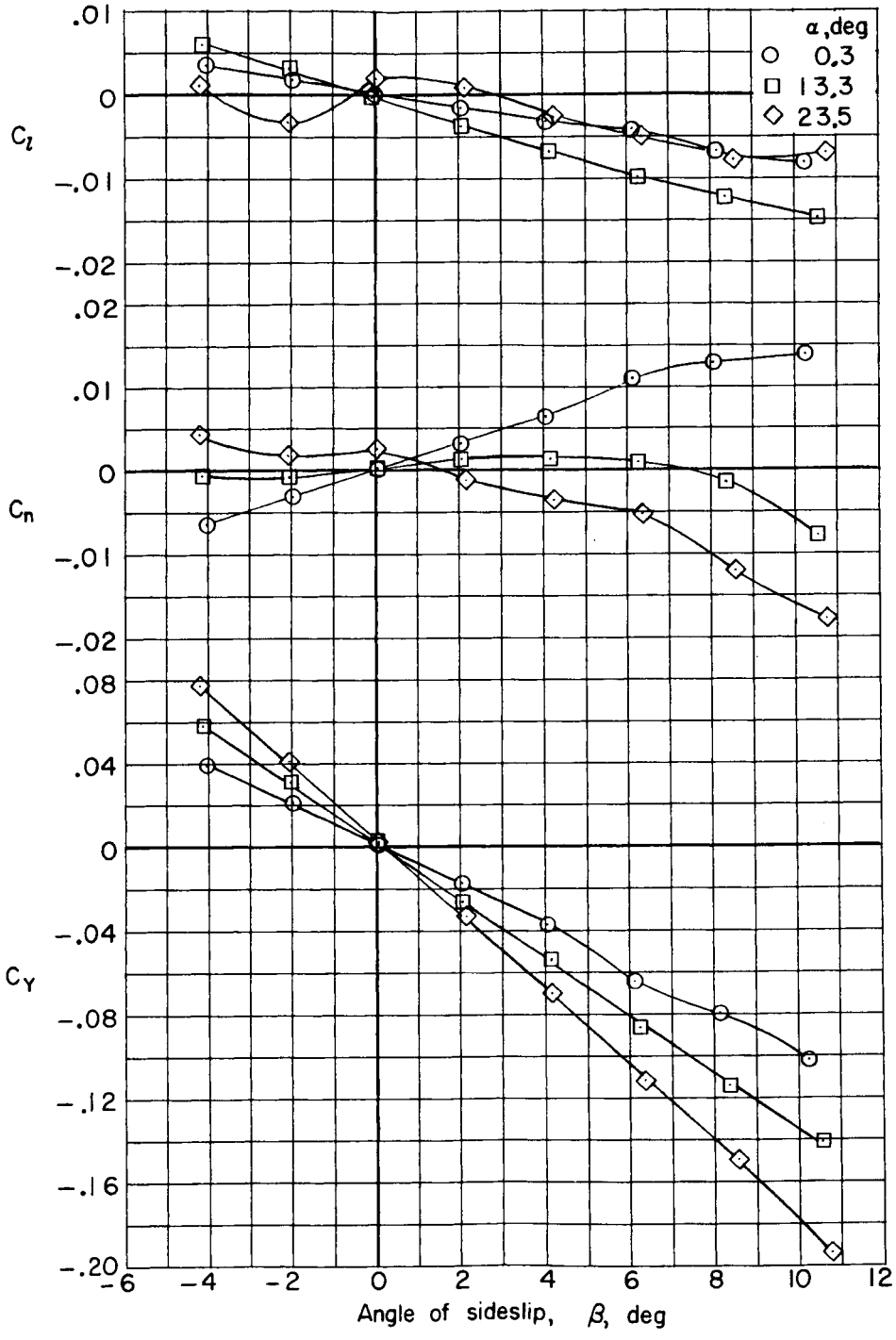

(a) M = 1.60.

Figure 7.- Lateral aerodynamic characteristics for the first stage at various angles of attack.

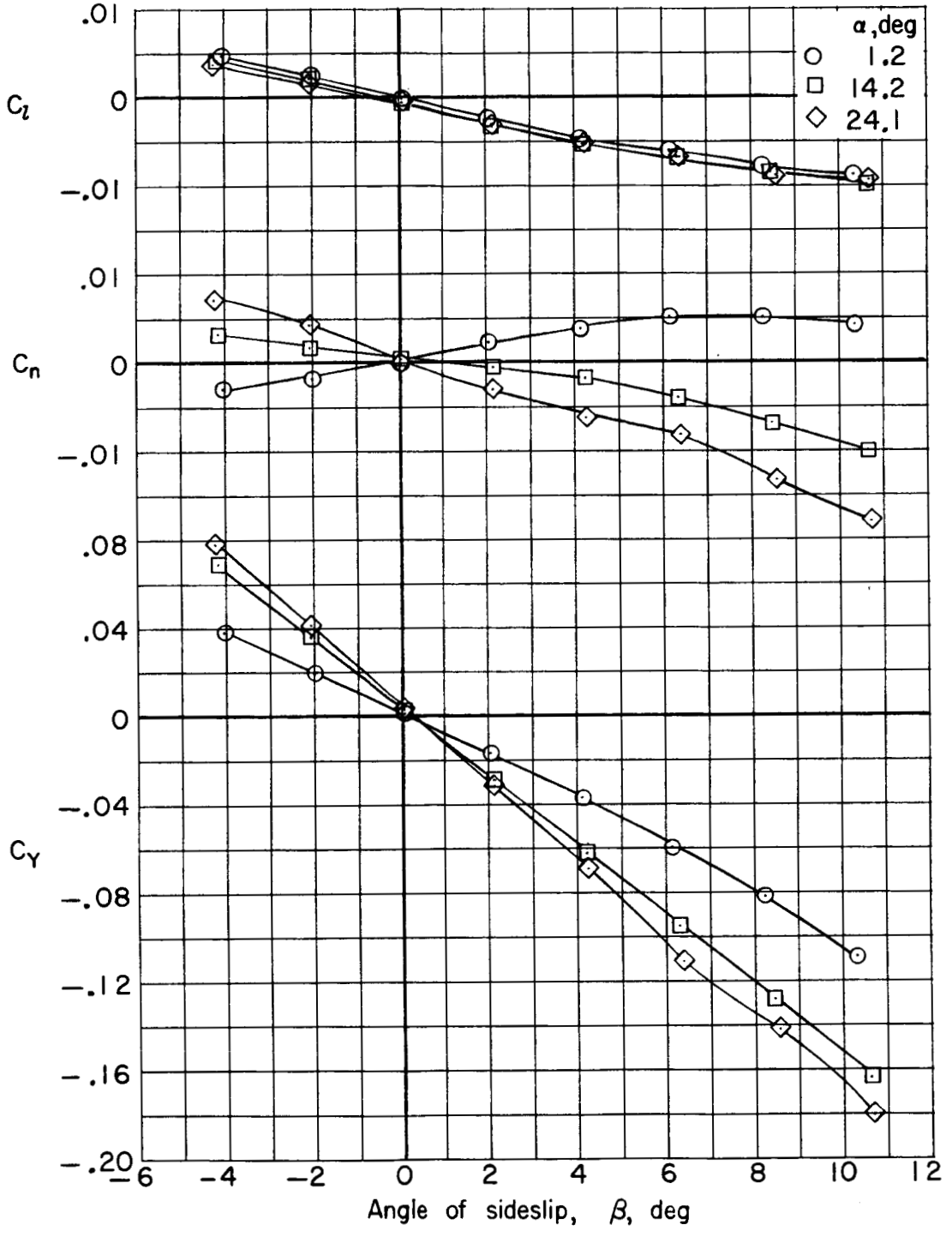

(b) M = 2.16.

Figure 7.- Continued.

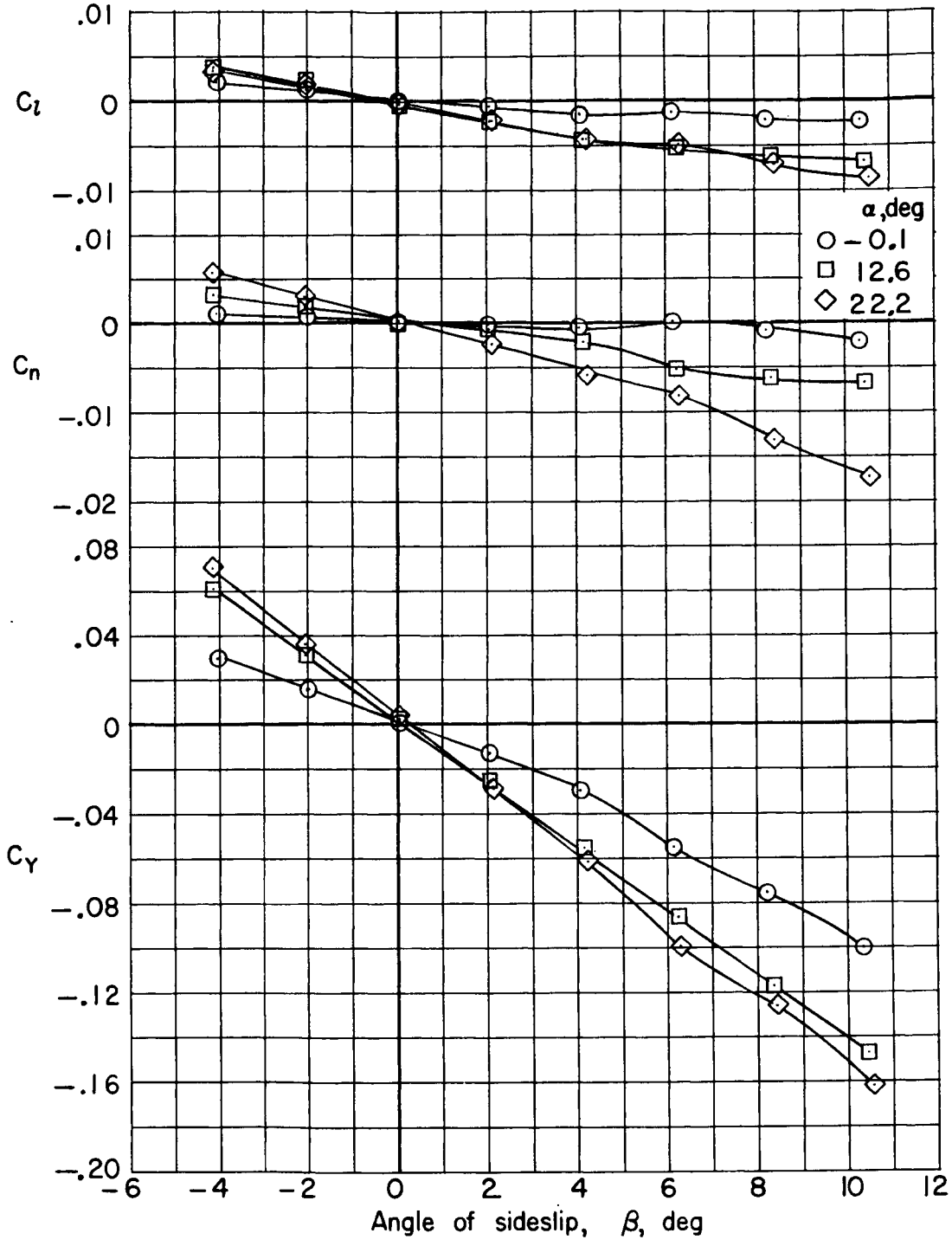

(c) M = 2.86.

Figure 7.- Concluded.

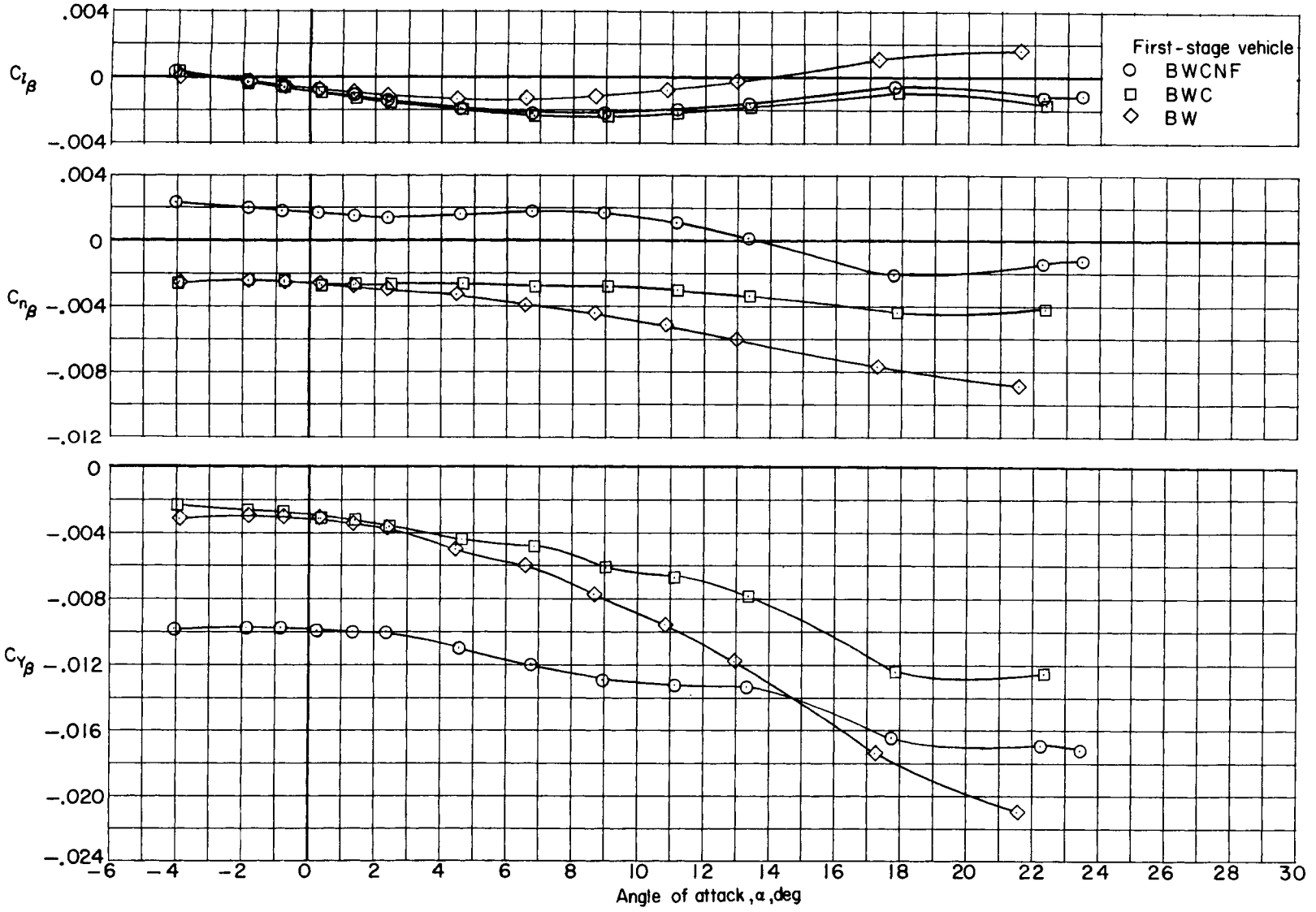

(a) M = 1.60.

Figure 8.- Variation with angle of attack of the lateral-directional-stability and side-force parameters for several first-stage configurations.

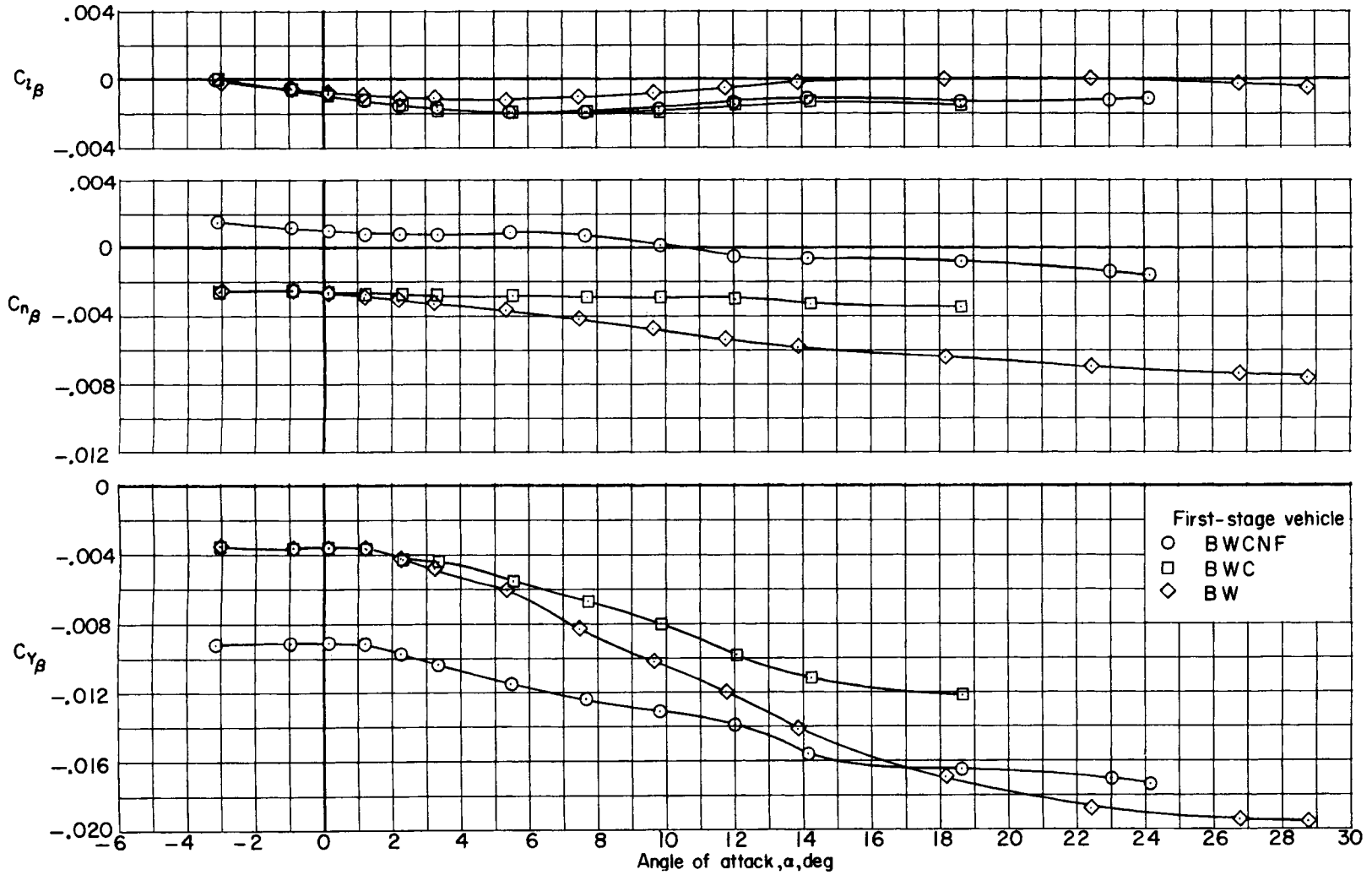

(b) M = 2.16.

Figure 8.- Continued.

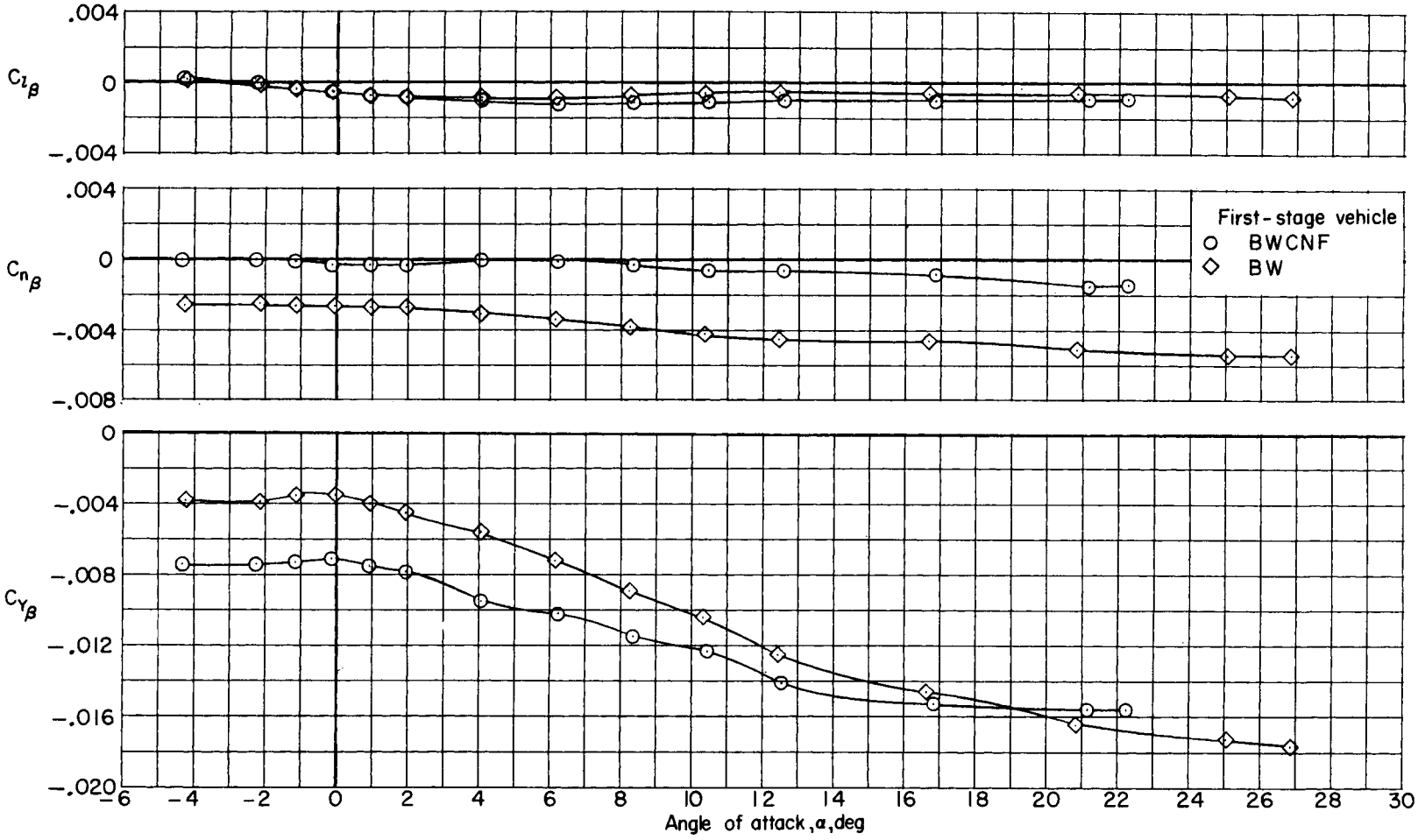

(c) M = 2.86.

Figure 8.- Concluded.

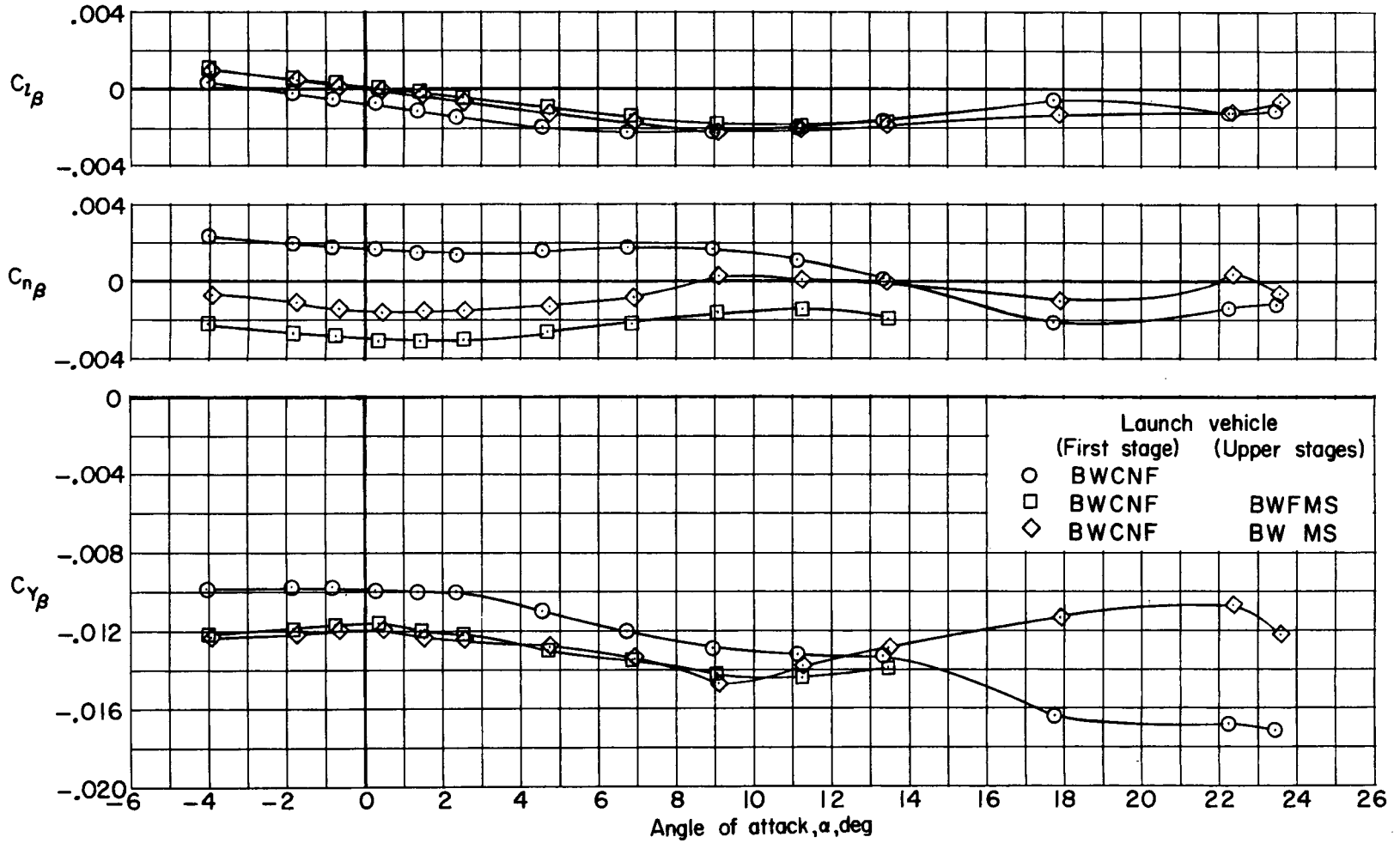

(a) M = 1.60.

Figure 9.- Variation with angle of attack of the lateral-directional-stability and side-force parameters for the complete launch vehicle with the effect of the maneuver propulsion package.

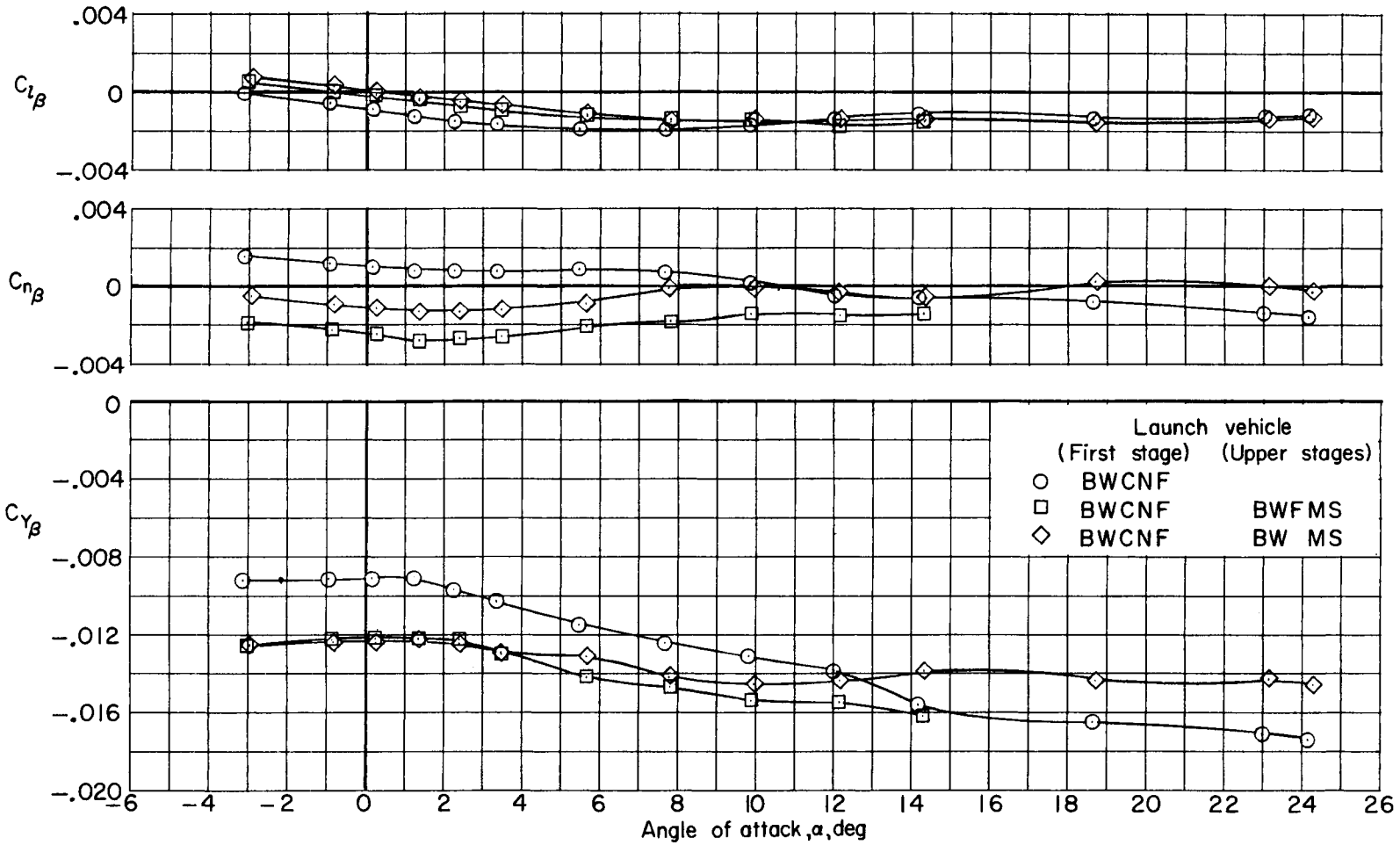

(b) M = 2.16.

Figure 9.- Continued.

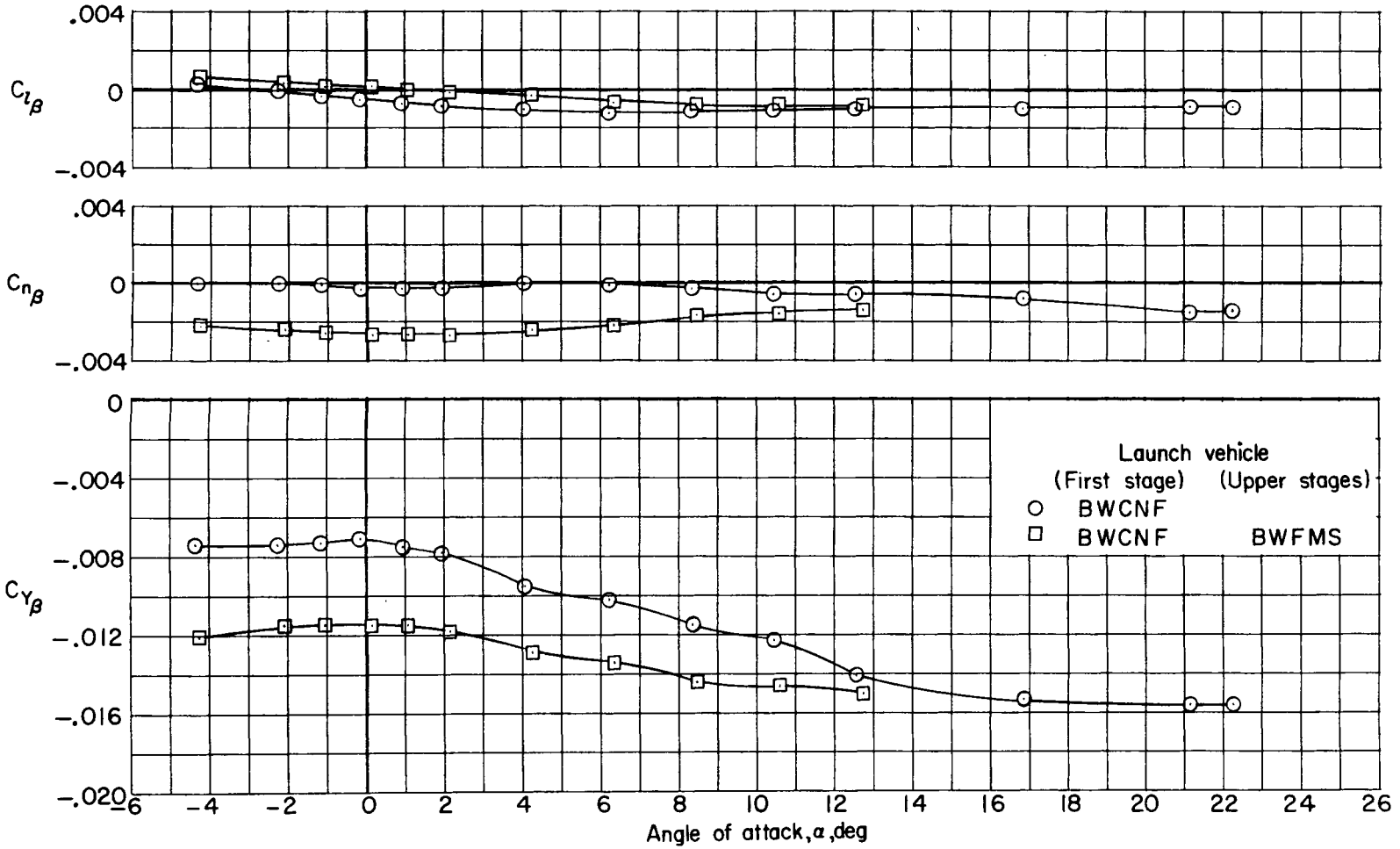

(c) M = 2.86.

Figure 9.- Concluded.

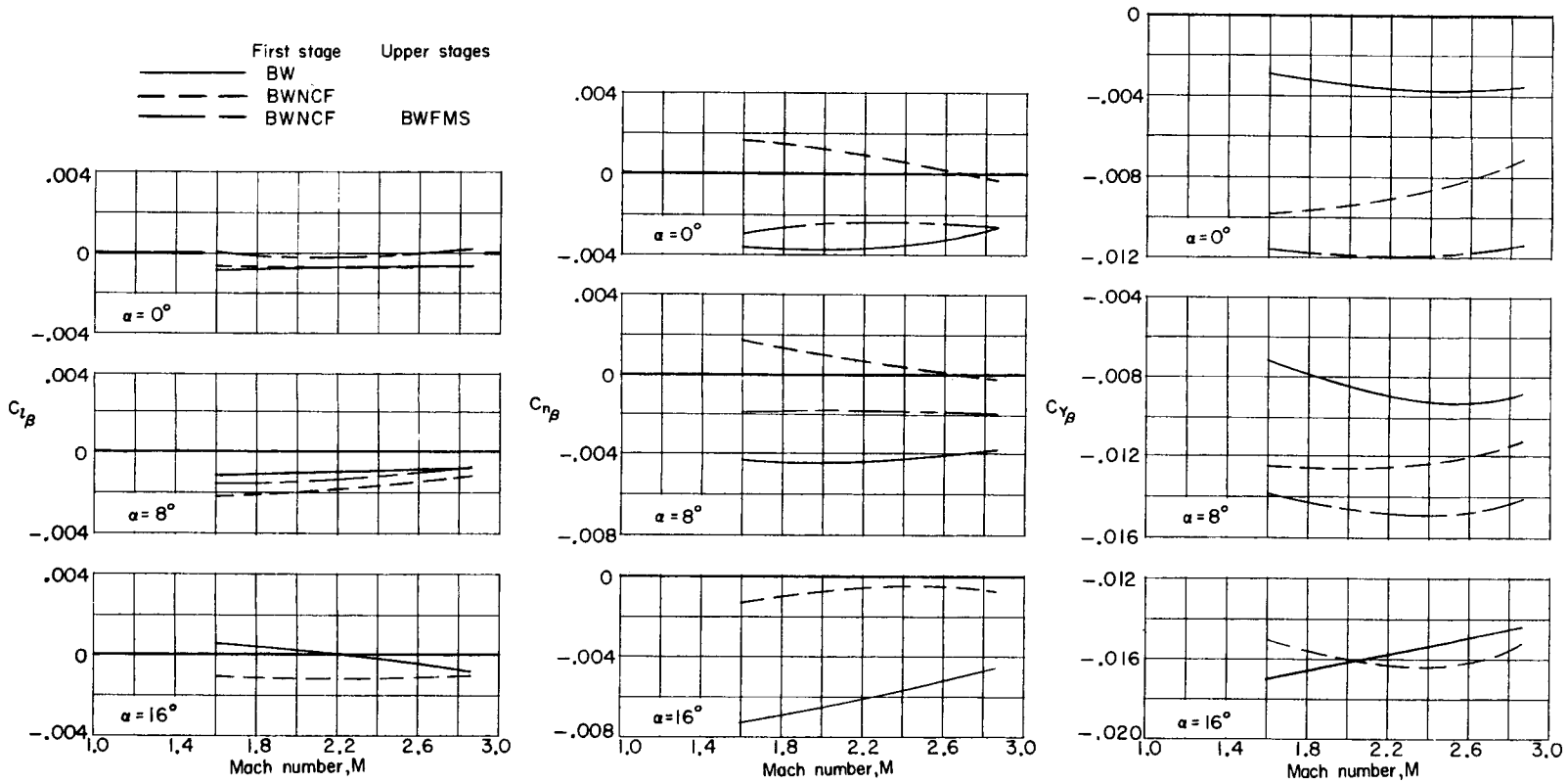

Figure 10.- Variation with Mach number of the lateral-directional-stability and side-force parameters for two first-stage configurations and the complete launch vehicle. $\alpha = 0^\circ$, 8°, and 16°.